MARVEL analysis of high-resolution rovibrational spectra of $^{16}O^{12}C^{18}O$

Dunia Alatoom [a,b,c], Mohammad Taha I. Ibrahim [a,b], Tibor Furtenbacher [d], Attila G. Császár [e], M. Alghizzawi[a,b], Sergei N. Yurchenko [b], Ala'a A. A. Azzam [a,c], Jonathan Tennyson [b,*]

[a]*AstroJo Institute, Wasfi Al-Tal St, Amman, Jordan*
[b]*Department of Physics and Astronomy, University College London, Gower Street, London WC1E 6BT, UK*
[c]*Department of Physics, The University of Jordan, Queen Rania St, Amman, Jordan*
[d]*HUN-REN–ELTE Complex Chemical Systems Research Group, H-1532 Budapest, P.O. Box 32, Hungary*
[e]*ELTE Eötvös Loránd University, Institute of Chemistry, H-1117 Budapest, Pázmány Péter sétány 1/A and HUN-REN–ELTE Complex Chemical Systems Research Group, H-1532 Budapest, P.O. Box 32, Hungary*

Abstract

8786 empirical rovibrational energy levels is presented for the third most abundant, asymmetric carbon dioxide isotopologue, $^{16}O^{12}C^{18}O$, based on a compiled dataset of experimental rovibrational transitions collected from the literature. The 53 literature sources utilized provide $19\,438$ measured lines with unique assignments in the wavenumber range of $2 - 12\,676$ cm^{-1}. The MARVEL (Measured Active Rotational-Vibrational Energy Levels) protocol, which is built upon the theory of spectroscopic networks, validates the great majority of these transitions and outputs 8786 empirical rovibrational energy levels with an uncertainty estimation based on the experimental uncertainties of the transitions. Issues found in the literature data, such as misassignment of quantum numbers, typographical errors, and misidentifications, are fixed before including them in the final MARVEL dataset and analysis. Comparison of the empirical energy-level data of this study with those in the line lists CDSD-2019 and Ames-2021 shows good overall agreement, significantly better for CDSD-2019; some issues raised by these comparisons are discussed.

Keywords: rovibrational energy levels, CO$_2$, line positions, MARVEL

---

1. Introduction

Numerous scientific and engineering domains, including atmospheric science [1], climate modeling [2], astrophysics [3], and gas laser technology [4, 5], benefit from knowledge about the high-resolution rovibrational spectroscopy of isotopologues of carbon dioxide, CO_2. Studying CO_2 in planetary atmospheres, including those of our neighbouring terrestrial planets, Venus [6] and Mars [7], provides insight into the time evolution of atmospheres [8]: a detailed understanding of how CO_2 abundance has changed over time on various planets sheds light on factors that influence the stability and composition of atmospheres.

Although CO_2 spectra are often dominated by the parent isotopologue [hereafter the original HITRAN isotopologue (AFGL, Air Force Geophysics Laboratory) shorthand codes, like 626 for $^{12}C^{16}O_2$, will be used], understanding fine details about the spectra of isotopologues of CO_2 is also highly relevant. To underline this statement, note that (a) isotopic abundances vary around the Universe and the isotopic composition of CO_2 is known to vary significantly in different regions of space, and (b) it is well established that the atmospheric absorptions on Earth associated with 626 are saturated (in other words, these lines are optically thick [9]), but this is not true in general for the other CO_2 isotopologues. Asymmetric CO_2 isotopologues, such as $^{16}O^{12}C^{18}O$ (628), are particularly important in this regard, since one of the effects of isotopic substitution is that it breaks the symmetry given by the two equivalent ^{16}O atoms in 626. This has significant consequences for the (ro)vibrational selection rules and as a result leads to new lines and shifts in the rovibrational spectra. Probably the most important effect of the isotopic substitution of one of the O atoms of carbon dioxide is that for 628 all rotational states are allowed, in contrast to 626 (or 636, which we have studied recently [10]), for which half of the states are forbidden by the Pauli principle. Thus, asymmetric isotopologues of CO_2 have significantly more spectral lines and, importantly, lines in ranges where 626 does not absorb.

The importance of the spectra of asymmetric CO_2 isotopologues has led to the development of theories to treat their vibrational motion [11] and the provision of rovibrational line lists of varying accuracy and size [12–15]. The rovibrational spectra of 628 have been studied using high-resolution and precision spectroscopic techniques [16–72]. These are the experimental studies considered in detail during this investigation.

The principal aim of the present computational study is the provision of large sets of validated measured line positions and accurate empirical rovibrational energies for 628. This is achieved through the use of the MARVEL (measured active rotational-vibrational energy levels) procedure [73–75], built upon the theory of spectroscopic networks [76, 77]. The datasets created during this study may also be used to improve theoretical models, can supplement variational nuclear-motion calculations, and improve line lists, like HITRAN [78] and ExoMol [79].

2. Theoretical Background

2.1. MARVEL

The MARVEL procedure [73–75] involves the careful identification and collection, the critical examination, and the thorough validation of high-resolution laboratory spectral data, with emphasis on the position of the lines. To be included in the MARVEL input file, a spectral line has to have not only an accurate position, but also unique labels for the upper and the lower energy levels and an associated uncertainty value. These spectral lines are then used to construct a spectroscopic network (SN), wherein each energy level serves as a vertex of the SN, and the vertices are interconnected with observed transitions (thus, they are the edges of the SN). This SN allows, *via* an inversion of the information contained in the measured lines, the determination of empirical energy-level values along with educated estimates for their uncertainties [80].

Ideally, one would create a well-connected SN linking all transitions to the ground state (the state with no rovibrational excitation, the root of the SN). However, due to the availability of incomplete experimental data, this is not usually feasible. In practice, the SN becomes fragmented, resulting in a principal component, where all the vertices are linked to the ground state, and a number of isolated, so-called floating components [81, 82]. The very nature of these floating components makes it uncertain whether their constituent lines align with all the other spectroscopic data, meaning that these lines remain "unvalidated" at the end of a MARVEL analysis. When floating components contain a substantial number of transitions, it may be desirable to connect them to the principal component(s) using accurate (semi-)empirical lines.

Since MARVEL is not constrained by detailed theoretical model assumptions, it is not affected by perturbations of energy levels caused by so-called accidental resonances. However, it can accept transitions that may be considered "illegal" (*e.g.*, not complying with well-established selection rules), as long as they are not in conflict with the rest of the data entering the analysis. Hence, it is crucial to continuously screen the experimental dataset for incorrect transitions during the construction of the MARVEL input. MARVEL can detect inconsistencies [82–84], that is lines which significantly deviate from the majority of the data provided. This feature proves invaluable for identifying issues with the experimental data, whether stemming from user mistakes during data collection and analysis or from misassignments.

2.2. Rovibrational quantum numbers

To ensure that MARVEL can successfully validate the measured transitions, labeling of the energy levels involved must be consistent across the entire dataset. In this work, as in our 636 study [10], we adopt the AFGL notation [85–87] for the description of the vibrational quantum states of CO_2. This notation uses five descriptors, v_1, v_2, l_2, v_3, and r, and avoids the use of super- and subscripts, and thus makes the notation well suited to electronic databases. In this notation the vibrational states are described by four quantum numbers and a counting number: v_1 and v_3 correspond to the "symmetric" and "antisymmetric" stretches, v_2 to the linear bend, l_2 is the angular momentum associated with the linear bending, and r is the so-called Fermi-resonance ranking index, which can range from 1 to $v_1 + 1$ [87–89]. In the 'standard' harmonic oscillator (HO) notation, $v_1 v_2^{l_2} v_3$, l_2 and v_3 are the same as in the AFGL notation. The AFGL notation can be related straightforwardly to the HO notation: for states mixed by the effects of Fermi-resonance, $v_1^{\text{AFGL}} = v_1^{\text{HO}} + (r - 1)$ and $v_2^{\text{AFGL}} = v_2^{\text{HO}} - 2(r - 1)$ [88]. Thus, for example, the state $2\,0^0\,0$ in HO notation corresponds to $2\,0\,0\,0\,1$ in AFGL, while $1\,2^0\,0 \equiv 2\,0\,0\,0\,2$ and $0\,4^0\,0 \equiv 2\,0\,0\,0\,3$ [90].

Besides the five vibrational descriptors utilized in the AFGL notation, there are two more descriptors characterizing a rovibrational quantum state of carbon dioxide, namely the rotational quantum number J and the rotationless parity p, the latter denoted here as either 'e' or 'f' [91]. Thus, the complete label of a rovibrational energy level adopted in this study is $(J\,v_1\,v_2\,l_2\,v_3\,r\,p)$. It is worth noting that in the AFGL notation the quantum numbers v_2 and l_2 are always equal [92]. The AFGL notation has the advantage, as shown by Amat and Pimbert [85], that while with the use of the standard notation the order of the rovibrational energy levels can change between isotopologues, in the AFGL notation this is not the case, though at the expense of the introduction of a redundant quantum number.

It must also be mentioned that besides Fermi resonances there are various other types of resonances affecting the infrared spectra of CO_2, such as Coriolis and ℓ-type resonances [93, 94]. These resonance effects contribute to the complexity of the spectral patterns and complicate the labeling of the energy levels. Nevertheless, Fermi resonances including overtones and combinations of the ν_1 and $2\nu_2$ states remain the most important interactions. Figure 1 illustrates the spectral ranges affected by Fermi resonances in the experimental spectrum. The effect is considerable across the entire spectrum, with some regions above 6000 cm^{-1} having up to six resonating bands.

2.3. Selection rules

For all asymmetric CO_2 isotopologues the equilibrium geometry belongs to the $C_{\infty v}$ point group. The selection rules for one-photon dipole-allowed rovibrational transitions among the quantum states of 628 can be summarized as follows. For rotational transitions, $\Delta J = 0, \pm 1$, and when
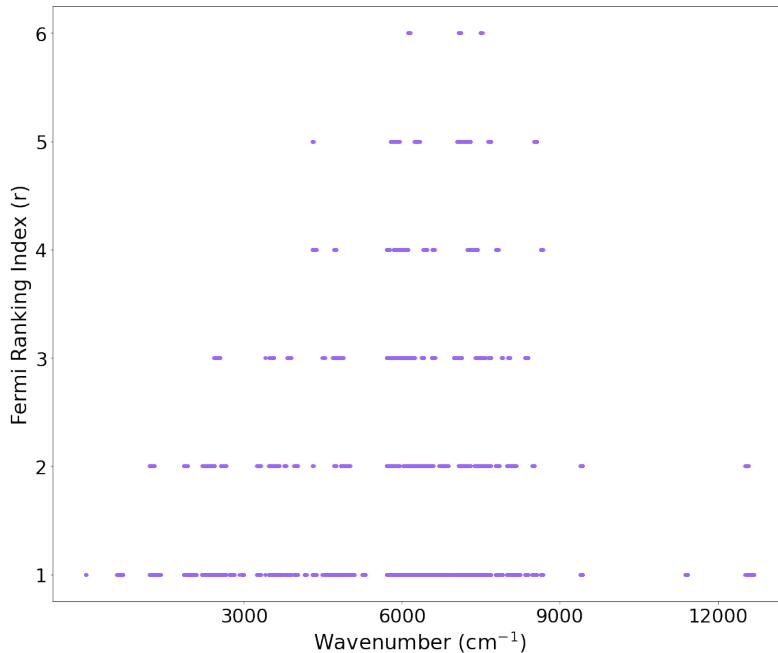

Figure 1: Distribution of the Fermi ranking index, r, of our final energy levels across the experimental spectral region covered.

$$\Delta J = 0; \quad \mathrm{e} \leftrightarrow \mathrm{f}, \tag{1}$$

that is the rotationless parity changes between the initial and the final states in the Q branch, while if

$$\Delta J = \pm 1; \quad \mathrm{e} \leftrightarrow \mathrm{e}, \mathrm{f} \leftrightarrow \mathrm{f}, \tag{2}$$

that is in the P and R branches there is no parity change. Furthermore, non-degenerate vibrational states with $l_2 = 0$ all have e parity (thus, in some sources the parity information is not given explicitly), while vibrational states with $l_2 > 0$ support both an e- and an f-parity state for each J.

2.4. Dataset construction

We closely follow the methodology described in our earlier study of the high-resolution spectroscopy of the 636 isotopologue of CO_2 [10]. Briefly, the method begins with a primary classification of the sources gathered, based on their experimental uncertainty, as well as the accuracy, self-consistency, and overall quality of the transitions reported. After a master dataset is built using data taken from the best sources, the rest of the sources are added carefully, while actively quarantining lines whose addition results in data conflicts. After this step, the quarantined lines are carefully inspected for possible errors, such as typos and misassignments. The errors detected are fixed and then the transition is added to the input dataset. The lines remaining under quarantine are removed from the final MARVEL analysis. These lines are marked with a minus sign in front of the wavenumber entry, as can be seen in the Supplementary Material.

After all the experimental data available are successfully included, or perhaps refuted, in the input dataset, a spectroscopic network is created from them. This SN, as usual, is fragmented, *i.e.*, it includes many floating components. In the case of carbon dioxide, including 628, the CDSD-2019 [14] line list contains results from accurate semi-empirical calculations; hence, we used transitions from this dataset to connect floating components to the principal one.

Following the inclusion of the majority of the observed transitions in the principal component, analysis of the uncertainties of the lines and then the energy levels was undertaken. Uncertainties of some of the lines have been increased based on recommendations of the MARVEL procedure, until self-consistency is achieved for the input dataset. This is followed by the generation of the empirical rovibrational energy levels. Finally, the empirical energy levels are compared to their counterparts in existing datasets [14, 15, 78], further searching for outliers. This last step also ensures the consistency of the energy-level labels across all datasets and identifies potential conflicts not detected by MARVEL.

3. Experimental Studies of $^{16}\mathrm{O}^{12}\mathrm{C}^{18}\mathrm{O}$ Line Positions

After a thorough search of the literature, we found 60 sources containing assigned experimental line positions for 628. Seven of these sources were assessed to be unusable and eventually were excluded from the MARVEL analysis. The specifics why these data are not used are discussed in Sec. 3.2. Characteristics of the 53 literature sources utilized, containing altogether 33 755 rovibrational transitions (19 438 unique ones), are summarized in Table 1. As detailed in Sec. 2.4, all the lines in the database underwent comprehensive processing and analysis, utilizing the fourth generation of the MARVEL code, which uses a bootstrap method to determine the uncertainty in the final energy levels [80]. Section 3.3 provides specific comments on some of the entries of Table 1.

3.1. Literature sources utilized

Tags for the literature sources of Table 1 were created following the practice introduced in Ref. 95. The first digits of the tag are the final two digits of the publication year of the article. This is followed by the two initial letters of the surname of each of the authors, limited to the first four authors. If the paper is written by a single author, the first eight letters of the complete surname is used. Each line is given a unique tag based on the reference tag and line counting number.

As to the experimental data, 12 362 transitions have been measured only once, while there are one and eight transitions which were measured ten and nine times, respectively. The principal component of the final SN contains 33 459 transitions, while the remaining 184 transitions form 112 floating components, containing 303 energy levels.

The experimentally measured transitions involve 9090 energy levels. We were able to determine empirical energies for 8786 rovibrational quantum states of 628. While in this study, and in our previous study of the high-resolution spectra of 636 [10], we have adopted the AFGL notation, several articles providing the transitions data utilized different notations, such as the standard (harmonic) notation. These sources can be identified *via* the last column of Table 1. In such cases and to make all datasets consistent, we matched the lines utilizing the HITRAN [78] and Ames-2021 [15] databases.

Figure 2 illustrates the distribution of the transitions data collected, using two vertical axes to help appreciate the amount of experimental data acquired compared to HITRAN 2020 [78]. One can clearly see that there is still a need for accurate experimental data across the spectrum.

Table 1: Experimental sources of rovibrational transitions of $^{16}O^{12}C^{18}O$ and some characteristics of the lines they contain.

Source	Range / cm^{-1}	A/V/D[a]	CSU[b]	MSU[c]	Notation
80EnYoSaHo[26]	2.21-5.89	5/5/0	1.7×10^{-6}	1.7×10^{-6}	Other
80PaKaAn[28]	624.52-702.51	118/118/0	1.2×10^{-3}	2.6×10^{-3}	Other
85Jolma[35]	632.90-696.32	92/91/1	5.0×10^{-4}	5.1×10^{-4}	Other
86GuRa[40]	644.22-2355.26	87/87/0	5.0×10^{-4}	5.2×10^{-4}	Other
86BrSoFr[96]	933.72-1094.35	98/98/0	4.3×10^{-7}	4.3×10^{-7}	Other
85Toth[37]	1212.73-1416.49	371/371/0	5.0×10^{-4}	5.3×10^{-4}	AFGL
83BeRiRiSo[29]	1859.38-1868.55	3/3/0	1.0×10^{-4}	1.0×10^{-4}	AFGL
85RiBeDe[36]	1859.38-1931.68	36/34/2	1.0×10^{-3}	1.1×10^{-3}	AFGL
84RiBeDeFe[34]	1862.90-2659.60	851/849/2	1.0×10^{-3}	1.6×10^{-3}	AFGL
12LyKaJaLu[54]	1865.02-6937.38	3372/3372/0	1.0×10^{-3}	1.2×10^{-3}	AFGL
84RiBe[33]	2004.91-2096.71	92/92/0	1.0×10^{-3}	1.3×10^{-3}	AFGL
12JaGuLyKa[53]	2019.93-5066.98	436/436/0	1.0×10^{-4}	1.3×10^{-4}	AFGL
86RiBeDe[41]	2068.89-2103.72	18/18/0	1.0×10^{-3}	1.8×10^{-3}	AFGL
83EsRo[30]	2200.87-2377.59	1042/1036/6	1.2×10^{-3}	1.5×10^{-3}	AFGL
86EsSaRoVa[39]	2213.38-3721.75	1347/1344/3	9.7×10^{-4}	1.8×10^{-3}	AFGL
84BaRo[31]	2268.99-2369.42	214/207/7	1.0×10^{-4}	3.0×10^{-4}	AFGL
15ElSuMi[60]	2270.11-2368.45	79/79/0	3.0×10^{-6}	3.2×10^{-6}	Other
78BaDeChRa[24]	2270.74-2367.06	219/219/0	3.0×10^{-3}	4.9×10^{-3}	Other
80Guelachv[27]	2288.26-2361.92	95/95/0	1.5×10^{-4}	4.9×10^{-4}	Other
68ObRaHaMc(P)[21]	2298.17-2359.68	88/83/5	2.9×10^{-2}	3.1×10^{-2}	Other
68ObRaHaMc(O)[21]	2298.19-2359.69	78/78/0	2.5×10^{-2}	3.0×10^{-2}	Other
84DeRiBe[32]	2398.34-2659.60	466/464/2	1.0×10^{-3}	1.5×10^{-3}	AFGL
07ToMiBrDe[45]	2458.74-6937.01	1548/1548/0	4.8×10^{-4}	5.0×10^{-4}	AFGL
78RoFiBuCa[25]	2485.42-2640.19	81/81/0	1.5×10^{-2}	1.7×10^{-2}	AFGL
08ViMuNoHe[6]	2962.23-3000.13	47/47/0	1.0×10^{-2}	1.3×10^{-2}	AFGL
14BoJaLyTa[57]	3239.74-4662.39	1576/1572/4	1.7×10^{-4}	3.5×10^{-4}	AFGL
88BeDeRiFe[42]	3290.58-3314.03	21/21/0	1.0×10^{-3}	2.1×10^{-3}	AFGL
71ObRa[22]	3526.20-3705.35	173/173/0	3.0×10^{-3}	7.3×10^{-3}	AFGL
65GoRo[97]	3549.25-3695.38	55/55/0	5.0×10^{-3}	6.8×10^{-3}	Other
08WaPeTaSo[48]	3816.94-8235.96	3434/3433/1	1.1×10^{-3}	1.5×10^{-3}	AFGL
16VaKoMoKa[65]	4298.32-4378.04	531/531/0	2.0×10^{-3}	2.3×10^{-3}	AFGL
22MaBoPeSo[71]	4477.19-4540.00	22/22/0	3.0×10^{-3}	3.0×10^{-3}	AFGL
99KsGiChBr[43]	4593.69-4660.99	69/69/0	1.0×10^{-3}	1.0×10^{-3}	AFGL
15BoJaLyTa[59]	4696.28-5286.92	849/848/1	1.9×10^{-4}	4.5×10^{-4}	AFGL
16BeDeSuBr[63]	4704.18-4933.17	632/559/73	1.7×10^{-3}	4.5×10^{-3}	AFGL
23FlCeCaKa[72]	4895.58-4913.17	2/2/0	1.2×10^{-7}	1.2×10^{-7}	AFGL
18KaCeMoKa[69]	5703.45-5878.71	1253/1253/0	1.1×10^{-3}	1.2×10^{-3}	AFGL
18CeKaMoKa[68]	5731.90-5878.59	540/540/0	1.0×10^{-3}	1.2×10^{-3}	AFGL
08PeKaPeTa[46]	5851.82-6937.40	852/852/0	2.1×10^{-3}	2.3×10^{-3}	AFGL
13KaCaMoBe[55]	5851.82-6937.40	6426/6425/1	1.0×10^{-3}	1.2×10^{-3}	AFGL
06PeKaRoPe[44]	5957.55-6832.25	443/443/0	1.5×10^{-3}	1.8×10^{-3}	AFGL
15JaBoLyTa[61]	6090.52-6283.26	150/150/0	3.0×10^{-4}	4.2×10^{-4}	AFGL
16DeBeSuBr[64]	6120.09-6151.99	45/45/0	6.7×10^{-4}	1.4×10^{-3}	AFGL
05MaMaRoPe[98]	6132.73-6496.25	593/589/4	3.0×10^{-3}	3.3×10^{-3}	AFGL
17KaKaTaPe[67]	6977.92-7913.89	3429/3429/0	1.0×10^{-3}	1.2×10^{-3}	AFGL
09KaSoCa[50]	7123.01-7650.24	375/375/0	5.0×10^{-4}	9.0×10^{-4}	AFGL
10SoKaTaPe[52]	7128.15-7650.24	369/369/0	1.1×10^{-3}	1.3×10^{-3}	AFGL
10CaSoMoPe[51]	7316.45-7478.78	17/17/0	8.0×10^{-4}	8.7×10^{-4}	AFGL
14KaKaTaPe[58]	7985.91-8235.93	548/548/0	1.0×10^{-3}	1.2×10^{-3}	AFGL
20KaKaCa[70]	8333.44-8678.90	182/182/0	5.0×10^{-4}	7.3×10^{-4}	AFGL
15PeSoSoLy[62]	9378.84-9427.02	41/41/0	9.9×10^{-3}	3.1×10^{-3}	AFGL
16SeSiLuBo[66]	11374.09-11422.29	43/43/0	9.9×10^{-3}	9.9×10^{-3}	AFGL
13PaLiLuLi[56]	12504.90-12676.68	132/132/0	3.5×10^{-3}	3.5×10^{-3}	AFGL

[a] A/V/D = Available / Validated / Deleted transitions.
[b] CSU = Average claimed source uncertainty.
[c] MSU = Average MARVEL-suggested source uncertainty.

3.2. Literature sources not utilized

Below we explain why we did not use the data reported in some of the sources during the present MARVEL analysis of the high-resolution spectra of $^{16}O^{12}C^{18}O$.

86EsRo [38]: The 473 transitions provided by this source are all included in the large compilation of experimental results of 86EsSaRoVa [39].

49GoMoMcPi [16]: The lines of this source, covering the region 4766–4924 cm^{-1}, have the claimed uncertainty of 0.07 cm^{-1}. This region is well covered by more recent sources having significantly higher accuracy, and no new energy levels are produced from this source.

64BeEg [17]: The lines of this source, covering the region 2012–4650 cm^{-1}, have the claimed uncertainty of 0.07 cm^{-1}. This region is well covered by more recent sources having significantly higher resolution, and no new energy levels are produced from this source.

67Hahn [20]: This source provides the same bands twice in two sets of tables, with the second set of tables switching the assigned branch. Our analysis shows that their Table I provides the correct assignments. The lines of this source, covering the region around 4.3 µm, have an uncertainty of 0.04 cm^{-1}. This region is well covered by more recent sources having significantly higher accuracy, and no new energy levels are produced from this source.

77SrFiKlIl [23]: This source gives two transitions detected in Raman spectra, which obey different selection rules compared to one-photon transitions. However, they were not used, as they are not fully assigned, *i.e.*, no band was provided, and they have a low accuracy of 0.05 cm^{-1}.
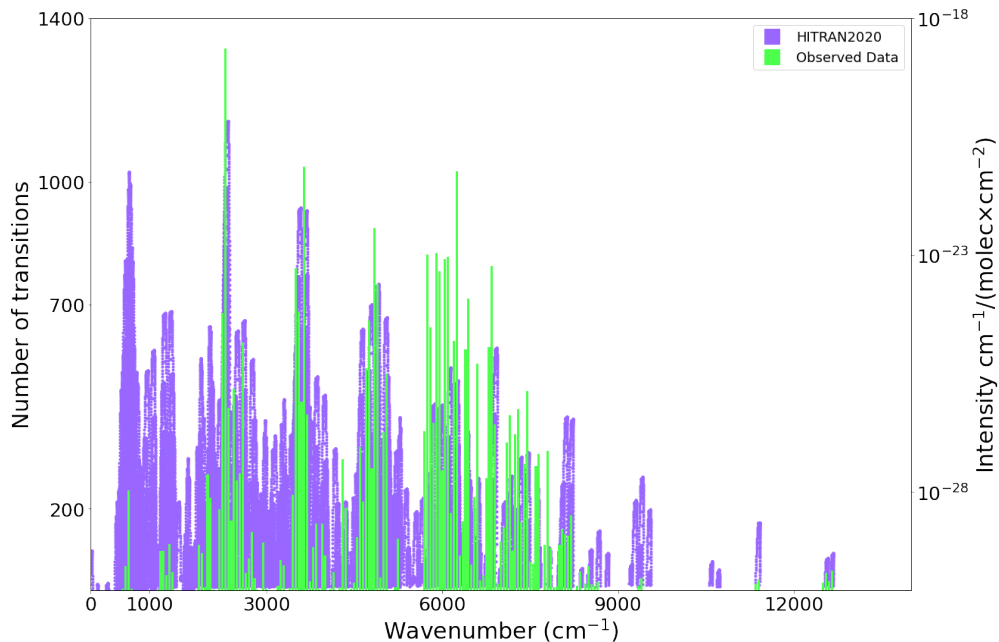
Figure 2: Coverage of the transitions data of $^{16}O^{12}C^{18}O$ obtained from literature sources (see Table 1 for more details about the sources). The green columns follow the left vertical axis and each column covers a region of 40 cm^{-1}. In the background, the spectrum from HITRAN 2020 [78] is given in purple, with the right vertical axis being the line intensity.

08ToBrMiDe [47]: The data provided is cited as coming from other sources; we acquired these data from their original sources.

08WiMaVaPe [49]: Transitions data reported in this source were detected in the atmosphere of Venus. These data need to go through further validation procedures to be included and used in a MARVEL-type analysis.

3.3. Specific comments on entries of Table 1

80EnYoSaHo [26]: This source contains five pure rotational transitions, whose measurement in the microwave region was made possible by the non-zero dipole moment, about $7.0(15) \times 10^{-4}$ D [26], of 628, arising due to the substitution of one ^{16}O with a ^{18}O atom in carbon dioxide.

68ObRaHaMc [21]: Two separate datasets were provided by two different laboratories, the two datasets were included independently. The dataset labeled 68ObRaHaMc(P) originates from the Pennsylvania laboratory, while the dataset labeled 68ObRaHaMc(O) comes from the Ohio laboratory.

78RoFiBuCa [25]: This source contains 81 transitions. Our MARVEL analysis suggested that these transitions need to be recalibrated. We found the calibration factor to be 0.999 972 29.

83EsRo [30]: Out of the 1042 measured transitions reported, 93 transitions could not be validated, as they form a number of floating components (thus, these transitions could still be correct).

66GoMc [19]: The data comes from the thesis 65Gordan [97].

86BrSoFr [96]: This paper presents beat-frequency measurements of transitions belonging to multiple isotopologues of carbon dioxide, as well as highly accurate calculated data in Tables III-XI. The beat-frequency measurements can not be utilized in our current study as they link transitions of different isotopologues. These high-accuracy data could potentially be useful after the construction of a 626 MARVEL set. We are in the process of constructing one. Our current study utilizes only the data presented in Table V of Ref. 96.

4. Results and Discussion

4.1. Relabeling of states

For the sake of unifying the notation of the quantum states of 628 across the entire dataset, we had to update the labels of slightly more than 1000 lines, collected from 11 sources (see Table 1). During the update, we found several lines whose assignment disagreed with the rest of the dataset. To check the assignments, these lines were compared to lines present in the Ames-2021 [15] and HITRAN 2020 [78] line lists.
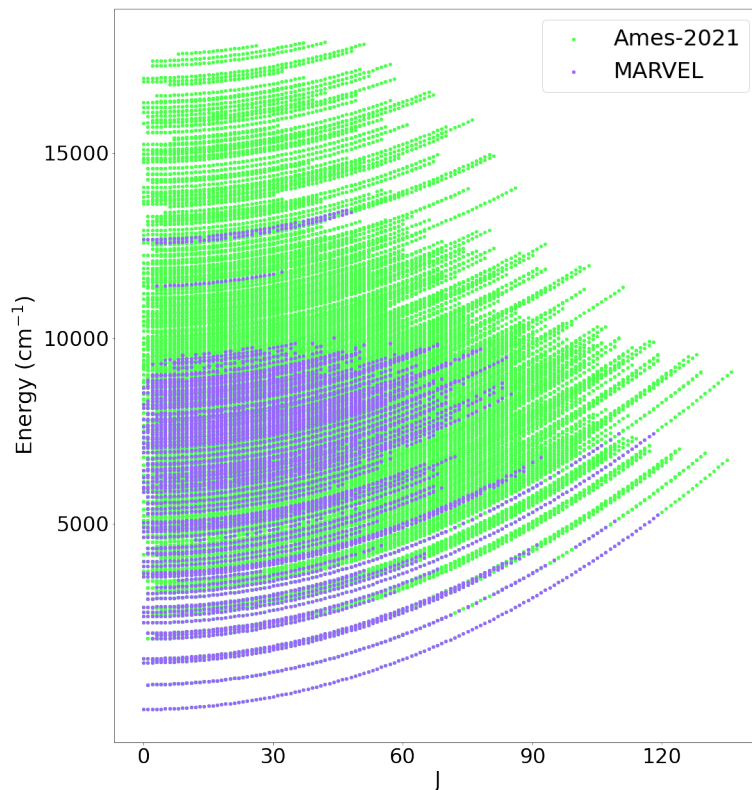
Figure 3: Energy-level coverage of the dataset obtained during this study against that of Ames-2021 [15]. See Table .3 (Appendix) for details about the vibrational bands of $^{16}O^{12}C^{18}O$.

4.2. Energy levels

As already noted above, our literature search ended up with 19 438 unique experimental transitions. During the validation process only slightly over 100 measured transitions had to be deleted, highlighting how careful the interpretations of high-resolution experimental measurements are for 628. Based on the validated transitions, MARVEL generated 8786 empirical rovibrational energy values. Figure 3 compares the energy-level coverage, as a function of the rotational quantum number J, of our experimental dataset and that of Ames-2021 [15]. Evidently, there is a lack of experimental data above $10\,000$ cm^{-1} and at high J values, especially above 7000 cm^{-1}. This calls for laboratory measurements at elevated temperatures.

Figure 4 illustrates the distribution of the transitions used for the determination of each empirical rovibrational energy level. Figure 4 reflects the fact that in experimental spectroscopic networks the degrees of the quantum states display an inverse-power-law-like (*i.e.*, heavy-tailed or near scale-free [99]) distribution [100, 101]. This distribution implies the presence of a small number of high-degree quantum states, called hubs, in the spectroscopic network, as clearly seen in this figure. The highest-degree hubs of $^{16}O^{12}C^{18}O$, which have more than 300 incident transitions, have the label (J 0 0 0 0 1 e), with $J = 13 - 17$, 25, and 27.

In Table .3 (see the Appendix), one finds information about specific vibrational bands. Note that the maximum value of J, $J_{max} = 119$, is for the 0 0 0 0 1 e ground vibrational state. The rotational coverage of the vibrationally excited bands is usually significantly less than this. The number of vibrational bands covered in this study is 190.

4.3. Comparison with line lists

Comparisons of our transitions and energy-level data with those in the available line lists, like CDSD-2019 [14] and Ames-2021 [15], show good overall agreement. Figures 5 and 6 show the absolute differences between the MARVEL data and those in CDSD-2019 and Ames-2021, respectively. It should be noted that our data show significantly better agreement with CDSD-2019 (0.0017 cm^{-1}) than with Ames-2021 (0.022 cm^{-1}), which is not surprising, since the CDSD-2019 data are semi-empirically fitted from experimental data.
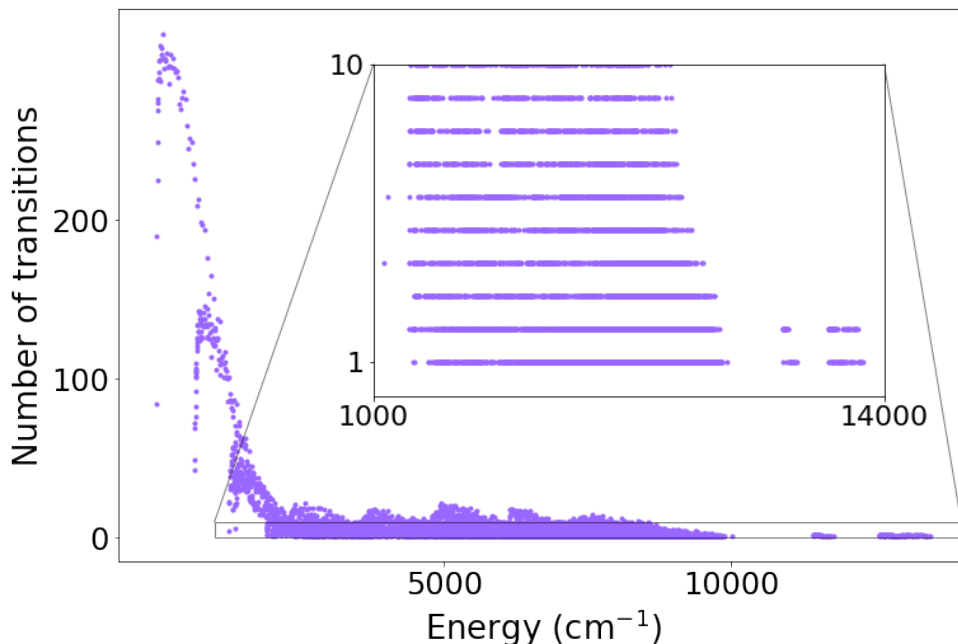
7

Figure 4: Degree distribution of the transitions used for the determination of empirical rovibrational energy level.

Table 2: Experimental energy levels with discrepancies larger than 0.1 cm^{-1} from the CDSD results.

MARVEL descriptors	MARVEL Energy / cm^{-1}	CDSD Energy / cm^{-1}	Difference / cm^{-1}	MARVEL unc /cm^{-1}	Comment
103 00011e	6231.4872	6231.3828	0.1044	8.423e-03	high-J energy level
104 00011e	6306.9318	6306.8290	0.1028	6.633e-03	high-J energy level
105 00011e	6383.0914	6382.9902	0.1012	8.966e-03	high-J energy level
106 00011e	6459.9729	6459.8663	0.1066	6.797e-03	high-J energy level
107 00011e	6537.5603	6537.4568	0.1035	8.953e-03	high-J energy level
108 00011e	6615.8710	6615.7615	0.1095	6.870e-03	high-J energy level
109 00011e	6694.8860	6694.7801	0.1059	9.017e-03	high-J energy level
110 00011e	6774.6247	6774.5123	0.1124	6.907e-03	high-J energy level
111 00011e	6855.0666	6854.9577	0.1089	9.040e-03	high-J energy level
112 00011e	6936.2314	6936.1161	0.1153	6.936e-03	high-J energy level
113 00011e	7018.0994	7017.9870	0.1124	9.420e-03	high-J energy level
114 00011e	7100.6886	7100.5706	0.1180	6.972e-03	high-J energy level
116 00011e	7267.9926	7267.8726	0.1200	7.246e-03	high-J energy level
35 51105f	7389.2683	7389.4869	0.2186	1.157e-03	mislabelled with 35 31112f
35 31112f	7389.4903	7389.2595	0.2309	1.157e-03	mislabelled with 35 51105f
118 00011e	7438.1397	7438.0201	0.1196	8.390e-03	high-J energy level
37 41113f	8638.2085	8638.0495	0.1589	1.744e-03	conflict: 13KaCaMoBe.5422 vs. CDSD
45 10031e	8964.4721	8964.6356	0.1635	2.027e-03	mislabelled in CDSD as 45 09911e

As shown in Fig. 5, there are energy levels with deviations from the CDSD results larger than 0.1 cm^{-1}. Table 2 lists these energy levels. It can be seen that most of these energy levels have high J rotational quantum number, where both the experimental and the effective Hamiltonian results are less reliable. Besides the trivial assignment conflicts, 35 31112f versus 35 51105f and 45 10031e versus 45 09911e, we found a notable issue: the experimental line position of 13KaCaMoBe.5422 is 6244.7874 cm^{-1}, while the same transition in CDSD has a line position of 6244.7732 cm^{-1}(the aforementioned line positions are not to be confused with the energy values presented in Table 2). Since the 13KaCaMoBe.5422 line is a single transition, MARVEL can not help to resolve this conflict. It is also important to note that we found several vibrational labels in the AMES database which contain double-digit quantum numbers, e.g., v_2=14, which is unusual for CO_2. These labels are not the same as the MARVEL labels; thus, these transitions have been excluded from the comparison presented.

5. Summary and Conclusions

This paper describes a comprehensive analysis, employing the MARVEL algorithm and code [73–75], of the high-resolution, rovibrational spectroscopy literature available for the third most abundant isotopologue of carbon dioxide, $^{16}O^{12}C^{18}O$. Assigned transitions have been extracted from altogether 53 literature sources (there are eight more sources

Figure 5: A comparison between rovibrational energies of the present dataset and those of CDSD-2019 [14], the unit is cm^{-1}. The average absolute difference between MARVEL and CDSD-2019 is as small as 0.0017 cm^{-1}. The maximum absolute difference between MARVEL and CDSD-2019 is 0.182 cm^{-1}.
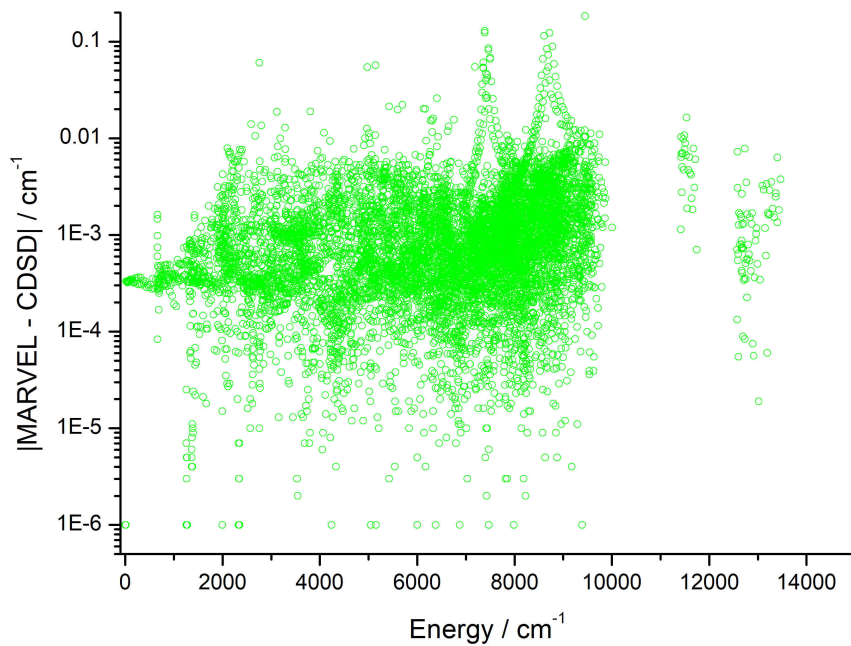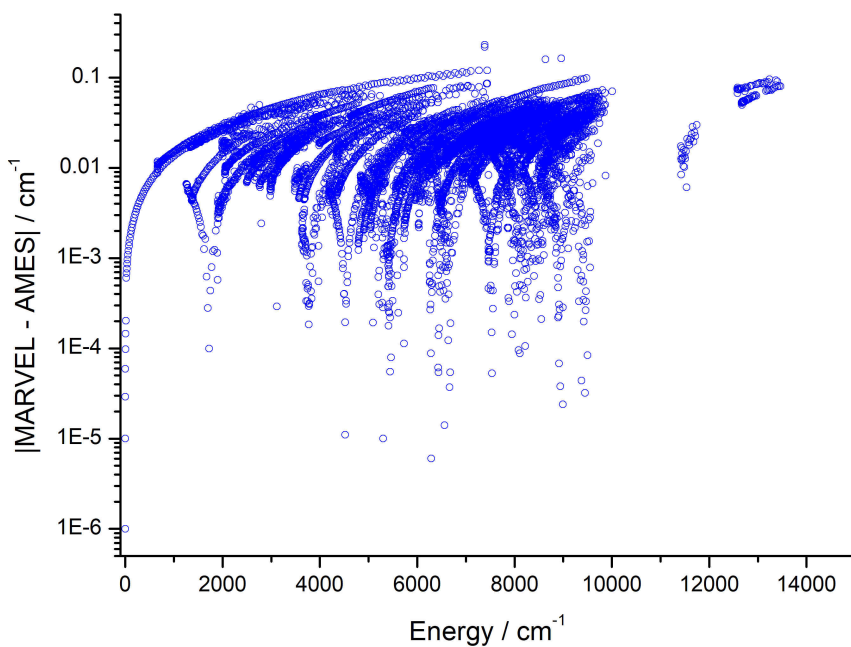

Figure 6: A comparison between rovibrational energies of the present dataset and those of Ames-2021 [15], the unit is cm^{-1}. The average absolute difference and the maximum absolute difference between MARVEL and Ames-2021 is 0.022 cm^{-1} and 0.230 cm^{-1}, respectively.

containing rovibrational transitions data about $^{16}O^{12}C^{18}O$ but for various reasons these data have not been utilized during the present study). The great majority of the transitions were verified using appropriate selection rules, tools provided by the network-theoretical algorithms MARVEL utilizes, and a comparative analysis against data available in the form of line lists. These extensive comparisons helped to ensure the consistency of the labelling of the quantum states involved in the measured transitions.

The transitions data validated for $^{16}O^{12}C^{18}O$ cover the wavenumber range of $2 - 12\,676$ cm^{-1}. The experimental transitions, of which there are $19\,438$ unique ones, yield 8786 empirical rovibrational energy levels. Estimates are provided for the uncertainties of the empirical energies, based on the experimental uncertainties of the transitions and the bootstrap technique. The detailed analysis of the present study reveals areas in the spectrum where there is a lack of experimental data.

Comparison with the CDSD-2019 database [14] reveals a small number of differences between the energy levels of the two databases. Most of the discrepancies are either for energy levels with high J rotational quantum number or energy levels defined by the 13KaCaMoBe [55] source. We do not know whether CDSD-2019 utilized this source or not. In the latter case we recommend that the next version of CDSD should include these measurement results. A comparison between our energy levels and those of Ames-2021 [15] and CDSD-2019 [14] shows significantly better agreement with CDSD-2019. This observation highlights the importance of fitting theoretical models using available experimental data.

There are plans to carry out further research in our groups to analyze, with the aid of the MARVEL procedure, more isotopologues of CO_2, including the parent one. These collectively will be used to give improved line lists for isotopologues of this important molecule.

Acknowledgements

Data availability

The MARVEL input file, including all the transitions, and the MARVEL output file, with all the energy levels, are supplied as Supplementary Material to this paper, which can be downloaded at ....

References

[1] J. M. Wallace, P. V. Hobbs, Atmospheric Science, 2nd ed., Elsevier, 2006. `doi:10.1016/c2009-0-00034-8`.

[2] N. Tanjeem, T. Kawazoe, T. Yatsui, CO_2 phonon mode renormalization using phonon-assisted energy up-conversion, Sci. Rep. 3 (2013) 3341. `doi:10.1038/srep03341`.

[3] E.-M. Ahrer, L. Alderson, N. M. Batalha, N. E. Batalha, J. L. Bean, T. G. Beatty, T. J. Bell, B. Benneke, Z. K. Berta-Thompson, A. L. Carter, I. J. M. Crossfield, N. Espinoza, A. D. Feinstein, J. J. Fortney, N. P. Gibson, J. M. Goyal, E. M.-R. Kempton, J. Kirk, L. Kreidberg, M. Lopez-Morales, M. R. Line, J. D. Lothringer, S. E. Moran, S. Mukherjee, K. Ohno, V. Parmentier, C. Piaulet, Z. Rustamkulov, E. Schlawin, D. K. Sing, K. B. Stevenson, H. R. Wakeford, N. H. Allen, S. M. Birkmann, J. Brande, N. Crouzet, P. E. Cubillos, M. Damiano, J.-M. Desert, P. Gao, J. Harrington, R. Hu, S. Kendrew, H. A. Knutson, P.-O. Lagage, J. Leconte, M. Lendl, R. J. MacDonald, E. M. May, Y. Miguel, K. Molaverdikhani, J. Moses, I, C. A. Murray, M. Nehring, N. K. Nikolov, D. J. M. P. D. de la Roche, M. Radica, P.-A. Roy, K. G. Stassun, J. Taylor, W. C. Waalkes, P. Wachiraphan, L. Welbanks, P. J. Wheatley, K. Aggarwal, M. K. Alam, A. Banerjee, J. K. Barstow, J. Blecic, S. L. Casewell, Q. Changeat, K. L. Chubb, K. D. Colon, L.-P. Coulombe, T. Daylan, M. De Val-Borro, L. Decin, L. A. Dos Santos, J. Flagg, K. France, G. Fu, A. G. Munoz, J. E. Gizis, A. Glidden, D. Grant, K. Heng, T. Henning, Y.-C. Hong, J. Inglis, N. Iro, T. Kataria, T. D. Komacek, J. E. Krick, E. K. H. Lee, N. K. Lewis, J. Lillo-Box, J. Lustig-Yaeger, L. Mancini, A. M. Mandell, M. Mansfield, M. S. Marley, T. Mikal-Evans, G. Morello, M. C. Nixon, K. O. Ceballos, A. A. A. Piette, D. Powell, B. Rackham, V, L. Ramos-Rosado, E. Rauscher, S. Redfield, L. K. Rogers, M. T. Roman, G. M. Roudier, N. Scarsdale, E. L. Shkolnik, J. Southworth, J. J. Spake, M. E. Steinrueck, X. Tan, J. K. Teske, P. Tremblin, S.-M. Tsai, G. S. Tucker, J. D. Turner, J. A. Valenti, O. Venot, I. P. Waldmann, N. L. Wallack, X. Zhang, S. Zieba, Identification of carbon dioxide in an exoplanet atmosphere, Nature 614 (2023) 649–652. `doi:10.1038/s41586-022-05269-w`.

[4] C. K. N. Patel, Selective excitation through vibrational energy transfer and optical maser action in N_2-CO_2, Phys. Rev. Lett. 13 (1964) 617–619. `doi:10.1103/physrevlett.13.617`.

[5] H. Foster, High power CO_2 lasers—a review, Opt. Laser Techn. 4 (1972) 121–128. `doi:10.1016/0030-3992(72)90018-7`.

[6] G. L. Villanueva, M. J. Mumma, R. E. Novak, T. Hewagama, Identification of a new band system of isotopic CO_2 near 3.3 μm: Implications for remote sensing of biomarker gases on Mars, Icarus 195 (2008) 34–44. `doi:10.1016/j.icarus.2007.11.014`.

10

[7] G. L. Villanueva, M. J. Mumma, R. E. Novak, T. Hewagama, Discovery of multiple bands of isotopic CO_2 in the prime spectral regions used when searching for CH_4 and HDO on Mars, J. Quant. Spectrosc. Radiat. Transf. 109 (2008) 883–894. doi:10.1016/j.jqsrt.2007.12.016.

[8] D. M. Hunten, Atmospheric evolution of the terrestrial planets, Science 259 (1993) 915–920.
URL http://www.jstor.org/stable/2880608

[9] K. P. Shine, G. E. Perry, Radiative forcing due to carbon dioxide decomposed into its component vibrational bands, Q. J. R. Meteorol. 149 (754) (2023) 1856–1866. doi:10.1002/qj.4485.

[10] M. T. I. Ibrahim, D. Alatoom, T. Furtenbacher, A. G. Csaszar, S. N. Yurchenko, A. A. A. Azzam, J. Tennyson, MARVEL analysis of high-resolution rovibrational spectra of $^{13}C^{16}O_2$, J. Comput. Chem. 45 (2024). doi:10.1002/jcc.27266.

[11] M. Bermudez-Montana, M. Rodriguez-Arcos, M. Carvajal, C. Ostertag-Henning, R. Lemus, A Spectroscopic Description of Asymmetric Isotopologues of CO2, J. Phys. Chem. A 127 (2023) 6357–6376. doi:10.1021/acs.jpca.3c00890.

[12] E. J. Zak, J. Tennyson, O. L. Polyansky, L. Lodi, N. F. Zobov, S. A. Tashkun, V. I. Perevalov, Room temperature line lists for CO_2 asymmetric isotopologues with *ab initio* computed intensities, J. Quant. Spectrosc. Radiat. Transf. 203 (2017) 265–281. doi:10.1016/j.jqsrt.2017.01.037.

[13] X. Huang, D. W. Schwenke, R. S. Freedman, T. J. Lee, Ames-2016 Line Lists for 13 Isotopologues of CO_2: Updates, Consistency, and Remaining Issues, J. Quant. Spectrosc. Radiat. Transf. 203 (2017) 224–241. doi:10.1016/j.jqsrt.2017.04.026.

[14] S. A. Tashkun, V. I. Perevalov, R. R. Gamache, J. Lamouroux, CDSD-296, high-resolution carbon dioxide spectroscopic databank: An update, J. Quant. Spectrosc. Radiat. Transf. 228 (2019) 124–131. doi:10.1016/j.jqsrt.2019.03.001.

[15] X. Huang, D. W. Schwenke, R. S. Freedman, T. J. Lee, Ames-2021 CO_2 dipole moment surface and IR line lists: Toward 0.1% uncertainty for CO_2 IR intensities, J. Phys. Chem. A 126 (35) (2022) 5940–5964, PMID: 36007245. doi:10.1021/acs.jpca.2c01291.

[16] L. Goldberg, O. C. Mohler, R. R. Mcmath, A. K. Pierce, Carbon dioxide in the infra-red solar spectrum, Phys. Rev. 76 (1949) 1848–1858. doi:10.1103/PhysRev.76.1848.

[17] C. V. Berney, D. F. E. Jr., Infrared Spectrum of Carbon Dioxide, Enriched in Oxygen-18, J. Chem. Phys. 40 (1964) 990–1000. doi:10.1063/1.1725293.

[18] H. R. Gordon, The infrared spectrum of CO_2 in the 2.8 and 15 micron regions, Ph.D. thesis, The Pennsylvania State University (1965).

[19] H. R. Gordon, T. K. McCubbin, The 2.8-micron bands of CO_2, J. Mol. Spectrosc. 19 (1966) 137–154. doi:10.1016/0022-2852(66)90237-2.

[20] Y. H. Hahn, The absorption and emission spectra of carbon-dioxide at 4.3 microns, Ph.D. thesis, The Pennsylvania State University (1967).
URL https://www.proquest.com/openview/074bf2696a7b47d2793ca1d620a02193/1?pq-origsite=gscholar&cbl=18750&diss=y

[21] R. Oberly, K. N. Rao, Y. H. Hahn, T. K. McCubbin, Bands of carbon dioxide in the region of 4.3 microns, J. Mol. Spectrosc. 25 (1968) 138–165. doi:10.1016/0022-2852(68)80002-5.

[22] R. Oberly, K. Narahari Rao, L. Jones, M. Goldblatt, Near infrared absorption spectra of Oxygen-18 Enriched Carbon Dioxide, J. Mol. Spectrosc. 40 (1971) 356–366. doi:10.1016/0022-2852(71)90160-3.

[23] K. Srinivasan, H. Finsterhölzl, H. W. Klöckner, D. Illig, H. W. Schrötter, Raman-spectroscopic observation of the σ-diads of $^{12}C^{16}O^{18}O$ and $^{12}C^{16}O^{17}O$, Z. Naturforsch. A 32 (1977) 1070–1071. doi:10.1515/zna-1977-0930.

[24] A. Baldacci, V. Malathy Devi, D.-W. Chen, K. Narahari Rao, B. Fridovich, Absorption spectrum of Carbon Dioxide at 4.3 μm, J. Mol. Spectrosc. 70 (1978) 143–159. doi:10.1016/0022-2852(78)90016-4.

[25] P. L. Roney, F. D. Findlay, H. L. Buijs, M. W. P. Cann, R. W. Nicholls, Carbon Dioxide spectral line frequencies for the 43-μm region, Appl. Opt. 17 (1978) 2599. doi:10.1364/AO.17.002599.

[26] Y. Endo, K. Yoshida, S. Saito, E. Horota, The microwave spectrum of Carbon Dioxide $-^{18}O$, Chem. Phys. 73 (7) (1980) 3511–3512. doi:10.1063/1.440509.

[27] G. Guelachvili, High-resolution fourier spectra of carbon dioxide and three of its isotopic species near 4.3 μm, J. Mol. Spectrosc. 79 (1980) 72–83. doi:10.1016/0022-2852(80)90293-3.

[28] R. Paso, J. Kauppinen, R. Anttila, Infrared spectrum of CO_2 in the region of the bending fundamental ν_2, J. Mol. Spectrosc. 79 (1980) 236–253. doi:10.1016/0022-2852(80)90304-5.

[29] C. P. Rinsland, D. C. Benner, V. Malathy Devi, P. S. Ferry, C. H. Sutton, D. J. Richardson, Atlas of high resolution infrared spectra of carbon dioxide, NASA, 1983.
URL https://scholarworks.wm.edu/aspubs/1047

[30] M. P. Esplin, L. S. Rothman, Spectral measurements of high temperature isotopic carbon dioxide in the 4.3 μm region, J. Mol. Spectrosc. 100 (1983) 193–204. doi:10.1016/0022-2852(83)90036-X.

[31] D. Bailly, C. Rossetti, $^{13}C^{16}O_2$, $^{13}C^{18}O_2$: Emission spectra in the 4.5-μm region, J. Mol. Spectrosc. 105 (1984) 229–245. doi:10.1016/0022-2852(84)90114-0.

[32] V. M. Devi, C. P. Rinsland, D. C. Benner, Absolute intensity measurements of CO_2 bands in the 2395–2680-cm^-1 region, Appl. Opt. 23 (22) (1984) 4067. doi:10.1364/AO.23.004067.

[33] C. P. Rinsland, D. C. Benner, Absolute intensities of spectral lines in carbon dioxide bands near 2050 cm^{-1}, Appl. Opt. 23 (1984) 4523–4528. doi:10.1364/AO.23.004523.

[34] C. P. Rinsland, D. C. Benner, V. M. Devi, P. S. Ferry, C. H. Sutton, D. J. Richardson, Atlas of high resolution infrared spectra of carbon dioxide, Appl. Opt. 23 (1984) 2051–2052. doi:10.1364/AO.23.002051.

[35] K. Jolma, Infrared spectrum of isotopic carbon dioxide in the region of bending fundamental ν_2, J. Mol. Spectrosc. 111 (1985) 211–218. doi:10.1016/0022-2852(85)90002-5.

[36] C. P. Rinsland, D. C. Benner, V. M. Devi, Measurements of absolute line intensities in carbon dioxide bands near 5.2 μm, Appl. Opt. 24 (1985) 1644–1650. doi:10.1364/AO.24.001644.

[37] R. A. Toth, Line positions and strengths of CO_2 in the 1200–1430-cm^-1 region, Appl. Opt. 24 (1985) 261. doi:10.1364/AO.24.000261.

[38] M. P. Esplin, L. S. Rothman, Spectral measurements of high-temperature isotopic carbon dioxide in the 4.5- and 2.8 μm regions, J. Mol. Spectrosc. 116 (1986) 351–363. doi:10.1016/0022-2852(86)90132-3.

[39] M. P. Esplin, H. Sakai, L. S. Rothman, G. A. Vanasse, W. M. Barowy, R. J. Huppi, Carbon dioxide line positions in the 2.8 and 4.3 micron regions at 800 Kelvin, Tech. Rep. AFGL-TR-86-0046, Utah State University (1986).
URL https://apps.dtic.mil/sti/citations/ADA173808

[40] G. Guelachvili, K. R. Rao, Handbook of Infrared Standards, Academic Press, 1986.

[41] C. P. Rinsland, D. C. Benner, V. M. Devi, Absolute line intensities in CO_2 bands near 4.8 μm, Appl. Opt. 25 (1986) 1204–1214.

doi:10.1364/AO.25.001204.

[42] D. C. Benner, V. M. Devi, C. P. Rinsland, P. S. Ferry-Leeper, Absolute intensities of CO_2 lines in the 3140-3410-cm^{-1} spectral region, Appl. Opt. 27 (1988) 1588–1597. doi:10.1364/AO.27.001588.

[43] R. J. Kshirsagar, L. P. Giver, C. Chackerian, L. R. Brown, The rovibrational intensities of the $2\nu_3$ band of $^{12}C^{16}O^{18}O$ at 4639 cm^{-1}, J. Quant. Spectrosc. Radiat. Transf. 61 (1999) 695–701. doi:10.1016/S0022-4073(98)00058-2.

[44] B. V. Perevalov, S. Kassi, D. Romanini, V. I. Perevalov, S. A. Tashkun, A. Campargue, CW-cavity ringdown spectroscopy of carbon dioxide isotopologues near 1.5 μm, J. Mol. Spectrosc. 238 (2006) 241–255. doi:10.1016/j.jms.2006.05.009.

[45] R. A. Toth, C. E. Miller, L. R. Brown, V. Malathy Devi, D. C. Benner, Line positions and strengths of $^{16}O^{12}C^{18}O$, $^{18}O^{12}C^{18}O$ and $^{17}O^{12}C^{18}O$ between 2200 and 7000 cm^{-1}, J. Mol. Spectrosc. 243 (2007) 43–61. doi:10.1016/j.jms.2007.03.005.

[46] B. V. Perevalov, S. Kassi, V. I. Perevalov, S. A. Tashkun, A. Campargue, High sensitivity CW-CRDS spectroscopy of $^{12}C^{16}O_2$, $^{16}O^{12}C^{17}O$ and $^{16}O^{12}C^{18}O$ between 5851 and 7045 cm^{-1}: Line positions analysis and critical review of the current databases, J. Mol. Spectrosc. 252 (2008) 143–159. doi:10.1016/j.jms.2008.06.012.

[47] R. A. Toth, L. R. Brown, C. E. Miller, V. M. Devi, D. C. Benner, Spectroscopic database of CO_2 line parameters: 4300–7000 cm^{-1}, J. Quant. Spectrosc. Radiat. Transf. 109 (2008) 906–921. doi:10.1016/j.jqsrt.2007.12.004.

[48] L. Wang, V. I. Perevalov, S. A. Tashkun, K.-F. Song, S.-M. Hu, Fourier transform spectroscopy of $^{12}C^{18}O_2$ and $^{16}O^{12}C^{18}O$ in the 3800–8500 cm^{-1} region and the global modeling of the absorption spectrum of $^{12}C^{18}O_2$, J. Mol. Spectrosc. 247 (2008) 64–75. doi:10.1016/j.jms.2007.09.015.

[49] V. Wilquet, A. Mahieux, A. C. Vandaele, V. I. Perevalov, S. A. Tashkun, A. Fedorova, O. Korablev, F. Montmessin, R. Dahoo, J.-L. Bertaux, Line parameters for the 01111–00001 band of 12C16O18O from SOIR measurements of the Venus atmosphere, J. Quant. Spectrosc. Radiat. Transf. 109 (2008) 895–905. doi:10.1016/j.jqsrt.2007.12.021.

[50] S. Kassi, K. F. Song, A. Campargue, High sensitivity CW-cavity ring down spectroscopy of $^{12}CO_2$ near 1.35 μm (I): line positions, J. Quant. Spectrosc. Radiat. Transf. 110 (2009) 1801–1814. doi:10.1016/j.jqsrt.2009.04.010.

[51] A. Campargue, K. F. Song, N. Mouton, V. I. Perevalov, S. Kassi, High sensitivity CW-Cavity Ring Down Spectroscopy of five $^{13}CO_2$ isotopologues of carbon dioxide in the 1.26-1.44 μm region (I): Line positions, J. Quant. Spectrosc. Radiat. Transf. 111 (2010) 659–674. doi:10.1016/j.jqsrt.2009.11.013.

[52] K. F. Song, S. Kassi, S. A. Tashkun, V. I. Perevalov, A. Campargue, High sensitivity CW-cavity ring down spectroscopy of $^{12}CO_2$ near 1.35 μm (II): New observations and line intensities modeling, J. Quant. Spectrosc. Radiat. Transf. 111 (2010) 332–344. doi:10.1016/j.jqsrt.2009.09.004.

[53] D. Jacquemart, F. Gueye, O. M. Lyulin, E. V. Karlovets, D. Baron, V. I. Perevalov, Infrared spectroscopy of CO_2 isotopologues from 2200 to 7000cm^{-1}: I—Characterizing experimental uncertainties of positions and intensities, J. Quant. Spectrosc. Radiat. Transf. 113 (11) (2012) 961–975. doi:10.1016/j.jqsrt.2012.02.020.

[54] O. M. Lyulin, E. V. Karlovets, D. Jacquemart, Y. Lu, A. W. Liu, V. I. Perevalov, Infrared spectroscopy of ^{17}O- and ^{18}O-enriched carbon dioxide in the 1700-8300 cm^{-1} wavenumber region, J. Quant. Spectrosc. Radiat. Transf. 113 (2012) 2167–2181. doi:10.1016/j.jqsrt.2012.06.028.

[55] E. V. Karlovets, A. Campargue, D. Mondelain, S. Béguier, S. Kassi, S. A. Tashkun, V. I. Perevalov, High sensitivity cavity ring down spectroscopy of ^{18}O enriched carbon dioxide between 5850 and 7000 cm^{-1}: I. Analysis and theoretical modeling of the $^{16}O^{12}C^{18}O$ spectrum, J. Quant. Spectrosc. Radiat. Transf. 130 (2013) 116–133. doi:10.1016/j.jqsrt.2013.05.019.

[56] H. Pan, X.-F. Li, Y. Lu, A.-W. Liu, V. Perevalov, S. Tashkun, S.-M. Hu, Cavity ring down spectroscopy of ^{18}O and ^{17}O enriched Carbon Dioxide near 795nm, J. Quant. Spectrosc. Radiat. Transf. 114 (2013) 42–44. doi:https://doi.org/10.1016/j.jqsrt.2012.08.017. URL https://www.sciencedirect.com/science/article/pii/S0022407312003925

[57] Y. G. Borkov, D. Jacquemart, O. M. Lyulin, S. A. Tashkun, V. I. Perevalov, Infrared spectroscopy of ^{17}O- and ^{18}O-enriched carbon dioxide: Line positions and intensities in the 3200–4700 cm^{-1} region. Global modeling of the line positions of $^{16}O^{12}C^{17}O$ and $^{17}O^{12}C^{17}O$, J. Quant. Spectrosc. Radiat. Transf. 137 (2014) 57–76. doi:10.1016/j.jqsrt.2013.11.008.

[58] E. V. Karlovets, S. Kassi, S. A. Tashkun, V. I. Perevalov, A. Campargue, High sensitivity cavity ring down spectroscopy of carbon dioxide in the 1.19-1.26 μm region, J. Quant. Spectrosc. Radiat. Transf. 144 (2014) 137–153. doi:10.1016/j.jqsrt.2014.04.001.

[59] Y. G. Borkov, D. Jacquemart, O. M. Lyulin, S. A. Tashkun, V. I. Perevalov, Infrared spectroscopy of ^{17}O- and ^{18}O-enriched carbon dioxide: Line positions and intensities in the 4681-5337 cm^{-1} region, J. Quant. Spectrosc. Radiat. Transf. 159 (2015) 1–10. doi:10.1016/j.jqsrt.2015.02.019.

[60] B. M. Elliott, K. Sung, C. E. Miller, FT-IR spectra of ^{18}O-, and ^{13}C-enriched CO_2 in the ν_3 region: High accuracy frequency calibration and spectroscopic constants for $^{16}O^{12}C^{18}O$, $^{18}O^{12}C^{18}O$, and $^{16}O^{13}C^{16}O$, J. Mol. Spectrosc. 312 (2015) 78–86. doi:10.1016/j.jms.2015.02.007.

[61] D. Jacquemart, Y. Borkov, O. Lyulin, S. Tashkun, V. Perevalov, Fourier transform spectroscopy of co$_2$ isotopologues at 1.6μm: Line positions and intensities, J. Quant. Spectrosc. Radiat. Transf. 160 (2015) 1–9. doi:https://doi.org/10.1016/j.jqsrt.2015.03.016. URL https://www.sciencedirect.com/science/article/pii/S0022407315001089

[62] T. M. Petrova, A. M. Solodov, A. A. Solodov, O. M. Lyulin, Y. G. Borkov, S. A. Tashkun, V. I. Perevalov, Measurements of CO_2 line parameters in the 9250–9500 cm^{-1} and 10,700–10,860 cm^{-1} regions, J. Quant. Spectrosc. Radiat. Transf. 164 (2015) 109–116. doi:10.1016/j.jqsrt.2015.06.001.

[63] D. C. Benner, V. M. Devi, K. Sung, L. R. Brown, C. E. Miller, V. H. Payne, B. J. Drouin, S. Yu, T. J. Crawford, A. W. Mantz, M. A. H. Smith, R. R. Gamache, Line parameters including temperature dependences of air- and self-broadened line shapes of $^{12}C^{16}O_2$: 2.06-μm region, J. Mol. Spectrosc. 326 (2016) 21–47, new Visions of Spectroscopic Databases, Volume I. doi:10.1016/j.jms.2016.02.012.

[64] V. M. Devi, D. C. Benner, K. Sung, L. R. Brown, T. J. Crawford, C. E. Miller, B. J. Drouin, V. H. Payne, S. Yu, M. A. H. Smith, A. W. Mantz, R. R. Gamache, Line parameters including temperature dependences of self- and air-broadened line shapes of $^{12}C^{16}O_2$: 1.6-μm region, J. Quant. Spectrosc. Radiat. Transf. 177 (2016) 117–144. doi:10.1016/j.jqsrt.2015.12.020.

[65] S. Vasilchenko, M. Konefal, D. Mondelain, S. Kassi, P. Čermák, S. A. Tashkun, V. I. Perevalov, A. Campargue, The CO_2 absorption spectrum in the 2.3 μm transparency window by high sensitivity CRDS: (I) Rovibrational lines, J. Quant. Spectrosc. Radiat. Transf. 184 (2016) 233–240. doi:10.1016/j.jqsrt.2016.07.002.

[66] V. Serdyukov, L. Sinitsa, A. Lugovskoi, Y. Borkov, S. Tashkun, V. Perevalov, Led-based fourier transform spectroscopy of $^{12}C^{16}O^{18}O$ and $^{12}C^{18}O_2$ in the 11,260–11,430 cm^{-1} range, J. Quant. Spectrosc. Radiat. Transf. 177 (2016) 145–151, xVIIIth Symposium on High Resolution Molecular Spectroscopy (HighRus-2015), Tomsk, Russia. doi:https://doi.org/10.1016/j.jqsrt.2015.11.024. URL https://www.sciencedirect.com/science/article/pii/S0022407315302132

[67] S. Kassi, E. V. Karlovets, S. A. Tashkun, V. I. Perevalov, A. Campargue, Analysis and theoretical modeling of the ^{18}O enriched carbon

dioxide spectrum by CRDS near 1.35 μm: (I) $^{16}O^{12}C^{18}O$, $^{16}O^{12}C^{17}O$, $^{12}C^{16}O_2$ and $^{13}C^{16}O_2$, J. Quant. Spectrosc. Radiat. Transf. 187 (2017) 414–425. doi:10.1016/j.jqsrt.2016.09.002.

[68] P. Čermák, E. V. Karlovets, D. Mondelain, S. Kassi, V. I. Perevalov, A. Campargue, High sensitivity CRDS of CO_2 in the 1.74 μm transparency window. A validation test for the spectroscopic databases, J. Quant. Spectrosc. Radiat. Transf. 207 (2018) 95–103. doi:10.1016/j.jqsrt.2017.12.018.

[69] E. Karlovets, P. Čermák, D. Mondelain, S. Kassi, A. Campargue, S. Tashkun, V. Perevalov, Analysis and theoretical modeling of the 18O enriched carbon dioxide spectrum by CRDS near 1.74 μm, J. Quant. Spectrosc. Radiat. Transf. 217 (2018) 73–85. doi:https://doi.org/10.1016/j.jqsrt.2018.05.017.
URL https://www.sciencedirect.com/science/article/pii/S0022407318302851

[70] E. V. Karlovets, S. Kassi, A. Campargue, High sensitivity CRDS of CO_2 in the 1.18 μm transparency window. Validation tests of current spectroscopic databases, J. Quant. Spectrosc. Radiat. Transf. 247 (2020) 106942. doi:10.1016/j.jqsrt.2020.106942.

[71] A. A. Marinina, Y. G. Borkov, T. M. Petrova, A. M. Solodov, A. A. Solodov, V. I. Perevalov, Absorption spectrum of carbon dioxide in the 4350-4550 cm^{-1} region, Atmos. Ocean. Opt. 35 (2022) 8–13. doi:10.1134/s1024856022010109.

[72] H. Fleurbaey, P. Čermák, A. Campargue, S. Kassi, D. Romanini, O. Votava, D. Mondelain, $^{12}CO_2$ transition frequencies with kHz-accuracy by saturation spectroscopy in the 1.99–2.09 μm region, Phys. Chem. Chem. Phys. 25 (2023) 16319–16330. doi:10.1039/D3CP01603J.

[73] A. G. Császár, G. Czakó, T. Furtenbacher, E. Mátyus, An active database approach to complete rotational–vibrational spectra of small molecules, Annu. Rep. Comput. Chem. 3 (2007) 155–176.

[74] T. Furtenbacher, A. G. Császár, J. Tennyson, MARVEL: measured active rotational–vibrational energy levels, J. Mol. Spectrosc. 245 (2007) 115–125. doi:10.1016/j.jms.2007.07.005.

[75] T. Furtenbacher, A. G. Császár, MARVEL: measured active rotational-vibrational energy levels. II. Algorithmic improvements, J. Quant. Spectrosc. Radiat. Transf. 113 (2012) 929–935. doi:10.1016/j.jqsrt.2012.01.005.

[76] A. G. Császár, T. Furtenbacher, Spectroscopic networks, J. Mol. Spectrosc. 266 (2011) 99 – 103. doi:10.1016/j.jms.2011.03.031.

[77] T. Furtenbacher, A. G. Császár, The role of intensities in determining characteristics of spectroscopic networks, Journal of Molecular Structure 1009 (2012) 123–129. doi:10.1016/j.molstruc.2011.10.057.

[78] I. E. Gordon, L. S. Rothman, R. J. Hargreaves, R. Hashemi, E. V. Karlovets, F. M. Skinner, E. K. Conway, C. Hill, R. V. Kochanov, Y. Tan, P. Wcisło, A. A. Finenko, K. Nelson, P. F. Bernath, M. Birk, V. Boudon, A. Campargue, K. V. Chance, A. Coustenis, B. J. Drouin, J. M. Flaud, R. R. Gamache, J. T. Hodges, D. Jacquemart, E. J. Mlawer, A. V. Nikitin, V. I. Perevalov, M. Rotger, J. Tennyson, G. C. Toon, H. Tran, V. G. Tyuterev, E. M. Adkins, A. Baker, A. Barbe, E. Canè, A. G. Császár, A. Dudaryonok, O. Egorov, A. J. Fleisher, H. Fleurbaey, A. Foltynowicz, T. Furtenbacher, J. J. Harrison, J. M. Hartmann, V. M. Horneman, X. Huang, T. Karman, J. Karns, S. Kassi, I. Kleiner, V. Kofman, F. Kwabia-Tchana, N. N. Lavrentieva, T. J. Lee, D. A. Long, A. A. Lukashevskaya, O. M. Lyulin, V. Y. Makhnev, W. Matt, S. T. Massie, M. Melosso, S. N. Mikhailenko, D. Mondelain, H. S. P. Müller, O. V. Naumenko, A. Perrin, O. L. Polyansky, E. Raddaoui, P. L. Raston, Z. D. Reed, M. Rey, C. Richard, R. Tóbiás, I. Sadiek, D. W. Schwenke, E. Starikova, K. Sung, F. Tamassia, S. A. Tashkun, J. Vander Auwera, I. A. Vasilenko, A. A. Vigasin, G. L. Villanueva, B. Vispoel, G. Wagner, A. Yachmenev, S. N. Yurchenko, The HITRAN2020 molecular spectroscopic database, J. Quant. Spectrosc. Radiat. Transf. 277 (2022) 107949. doi:10.1016/j.jqsrt.2021.107949.

[79] J. Tennyson, S. N. Yurchenko, ExoMol: molecular line lists for exoplanet and other atmospheres, Mon. Not. R. Astron. Soc. 425 (2012) 21–33. doi:10.1111/j.1365-2966.2012.21440.x.

[80] J. Tennyson, T. Furtenbacher, S. N. Yurchenko, A. G. Császár, Empirical rovibrational energy levels for nitrous oxide, J. Quant. Spectrosc. Radiat. Transf. 316 (2024) 108902. doi:10.1016/j.jqsrt.2024.108902.

[81] T. Furtenbacher, P. Árendás, G. Mellau, A. G. Császár, Simple molecules as complex systems, Sci. Rep. 4 (2014) 4654.

[82] A. G. Csaszar, T. Furtenbacher, P. Arendas, Small Molecules-Big Data, J. Phys. Chem. A 120 (2016) 8949–8969. doi:10.1021/acs.jpca.6b02293.

[83] R. Tóbiás, T. Furtenbacher, A. G. Császár, Cycle basis to the rescue, J. Quant. Spectrosc. Rad. Transfer 203 (2017) 557–564.

[84] P. Arendas, T. Furtenbacher, A. G. Csaszar, From bridges to cycles in spectroscopic networks, Sci. Rep. 10 (2020) 19489. doi:{10.1038/s41598-020-75087-5}.

[85] G. Amat, M. Pimbert, On Fermi resonance in carbon dioxide, J. Mol. Spectrosc. 16 (1965) 278–290. doi:10.1016/0022-2852(65)90123-2.

[86] L. S. Rothman, L. D. G. Young, Infrared energy levels and intensities of carbon dioxide-II, J. Quant. Spectrosc. Radiat. Transf. 25 (1981) 505–524. doi:10.1016/0022-4073(81)90026-.
URL https://doi.org/10.1016/0022-4073(81)90026-1

[87] R. A. Toth, L. R. Brown, C. E. Miller, V. Malathy Devi, D. C. Benner, Spectroscopic database of CO_2 line parameters: $4300 - 7000$ cm^{-1}, J. Quant. Spectrosc. Radiat. Transf. 109 (2008) 906–921. doi:10.1016/j.jqsrt.2007.12.004.

[88] R. A. McClatchey, W. S. Benedict, S. A. Clough, D. E. Burch, R. F. Calfee, K. Fox, L. S. Rothman, J. S. Garing, AFCRL atmospheric absorption line parameters compilation, Tech. Rep. AFCRL-TR-73-0096, Air Force Cambridge Research Laboratories (1983).
URL https://modis-images.gsfc.nasa.gov/JavaHAWKS/AFCRL_AALPC.pdf

[89] A. Baldacci, C. P. Rinsland, M. A. H. Smith, K. N. Rao, Spectrum of $^{13}C^{16}O_2$ at 2.8 μm, J. Mol. Spectrosc. 94 (1982) 351–362. doi:10.1016/0022-2852(82)90011-X.

[90] L. S. Rothman, L. D. G. Young, Infrared energy levels and intensities of carbon dioxide—ii, J. Quant. Spectrosc. Radiat. Transf. 25 (6) (1981) 505–524. doi:10.1016/0022-4073(81)90026-1.

[91] J. M. Brown, J. T. Hougen, K. P. Huber, J. W. C. Johns, I. Kopp, H. Lefebvre-Brion, A. J. Merer, D. A. Ramsay, J. Rostas, R. N. Zare, Labeling of parity doublet levels in linear molecules, J. Mol. Spectrosc. 55 (1975) 500–503. doi:10.1016/0022-2852(75)90291-X.

[92] M. P. Esplin, R. J. Huppi, H. Sakai, G. A. Vanasse, L. S. Rothman, Absorption measurements of CO_2 and H_2O at high resolution and elevated temperatures, Tech. Rep. AFGL-TR-82-0057, Utah State University (1982).
URL https://apps.dtic.mil/sti/citations/ADA113824

[93] W. D. Allen, Y. Yamaguchi, A. G. Császár, D. A. Clabo Jr., R. B. Remington, H. F. Schaefer III, A systematic study of molecular vibrational anharmonicity and vibration-rotation interaction by self-consistent-field higher derivative methods. Linear polyatomic molecules, Chem. Phys. 145 (1990) 427–466.

[94] B. Perevalov, Le spectre d'absorption du dioxyde de carbone dans le proche infrarouge (1.4-1.7 μm) : Cavity Ring Down Spectroscopy, modélisation globale et bases de données, Theses, Université Joseph-Fourier - Grenoble I (Feb. 2009).
URL https://theses.hal.science/tel-00600074

[95] J. Tennyson, P. F. Bernath, L. R. Brown, A. Campargue, M. R. Carleer, A. G. Császár, R. R. Gamache, J. T. Hodges, A. Jenouvrier, O. V. Naumenko, O. L. Polyansky, L. S. Rothman, R. A. Toth, A. C. Vandaele, N. F. Zobov, L. Daumont, A. Z. Fazliev, T. Furtenbacher, I. E. Gordon, S. N. Mikhailenko, S. V. Shirin, IUPAC critical evaluation of the rotational-vibrational spectra of water vapor. Part I. Energy levels and transition wavenumbers for $H_2^{17}O$ and $H_2^{18}O$, J. Quant. Spectrosc. Radiat. Transf. 110 (2009) 573–596. doi:10.1016/j.jqsrt.2009.02.014.

[96] L. Bradley, K. Soohoo, C. Freed, Absolute frequencies of lasing transitions in nine CO_2 isotopic species, IEEE J. Quantum Electron. 22 (1986) 234–267. doi:10.1109/JQE.1986.1072967.

[97] H. R. Gordon, The infrared spectrum of CO_2 in the 2.8 and 15 micron regions, Ph.D. thesis, The Pennsylvania State University (1965). URL https://www.proquest.com/openview/59dcaa567b3cb6b908786d3699a70cc9/1?pq-origsite=gscholar&cbl=18750&diss=y

[98] Z. Majcherova, P. Macko, D. Romanini, V. I. Perevalov, S. A. Tashkun, J.-L. Teffo, A. Campargue, High-sensitivity CW-cavity ringdown spectroscopy of $^{12}CO_2$ near 1.5 µm, J. Mol. Spectrosc. 230 (2005) 1–21. doi:10.1016/j.jms.2004.09.011.

[99] M. E. J. Newman, Networks, Oxford University Press, Oxford, 2010.

[100] T. Furtenbacher, P. Árendás, G. Mellau, A. G. Császár, Simple molecules as complex systems, Sci. Rep. 4 (2014) 4654. doi:10.1038/srep04654.

[101] A. G. Császár, T. Furtenbacher, P. Árendás, Small Molecules-Big Data, J. Phys. Chem. A 120 (2016) 8949–8969. doi:10.1021/acs.jpca.6b02293.

Table .3: Vibrational bands of $^{16}O^{12}C^{18}O$ investigated in this study with an ordering based on band descriptors.

Band	Range of J	Nb. of energy levels	Unc. range/cm^{-1}	Avg. unc./cm^{-1}	Range of energy levels/cm^{-1}
0 0 0 0 1 e	0 − 119	120	0.0000 − 0.0096	0.0020	0.0000 − 5233.4864
0 0 0 1 1 e	0 − 118	119	0.0000 − 0.0091	0.0019	2332.1126 − 7438.1397
0 0 0 2 1 e	0 − 68	69	0.0000 − 0.0012	0.0002	4639.5011 − 6337.2420
0 0 0 3 1 e	0 − 84	85	0.0003 − 0.0035	0.0008	6922.1967 − 9483.0059
0 0 0 4 1 e	7 − 41	22	0.0010 − 0.0011	0.0010	9200.2034 − 9793.9610
0 0 0 5 1 e	3 − 32	28	0.0080 − 0.0160	0.0083	11417.8923 − 11787.0476
0 1 1 0 1 e	1 − 109	93	0.0005 − 0.0093	0.0019	663.1091 − 5064.6047
0 1 1 0 1 f	1 − 104	89	0.0005 − 0.0082	0.0016	663.1132 − 4679.1109
0 1 1 1 1 e	1 − 110	92	0.0005 − 0.0096	0.0021	2982.8414 − 7429.8112
0 1 1 1 1 f	1 − 105	88	0.0005 − 0.0082	0.0017	2982.8434 − 7043.7292
0 1 1 2 1 e	1 − 46	45	0.0005 − 0.0017	0.0007	5277.8754 − 6061.0981
0 1 1 2 1 f	1 − 43	42	0.0005 − 0.0016	0.0006	5277.8793 − 5964.2518
0 1 1 3 1 e	1 − 76	71	0.0010 − 0.0064	0.0014	7548.2468 − 9650.1290
0 1 1 3 1 f	1 − 74	69	0.0010 − 0.0032	0.0013	7548.2480 − 9544.6214
0 2 2 0 1 e	2 − 78	75	0.0005 − 0.0057	0.0017	1327.3639 − 3597.5626
0 2 2 0 1 f	2 − 88	69	0.0008 − 0.0068	0.0022	1327.3640 − 4212.0507
0 2 2 1 1 e	2 − 79	73	0.0007 − 0.0056	0.0020	3634.7302 − 5945.0836
0 2 2 1 1 f	2 − 87	68	0.0012 − 0.0067	0.0024	3634.7302 − 6432.8821
0 2 2 3 1 e	2 − 59	55	0.0011 − 0.0058	0.0019	8175.4856 − 9449.7232
0 2 2 3 1 f	2 − 59	51	0.0016 − 0.0040	0.0020	8175.4856 − 9449.7346
0 3 3 0 1 e	3 − 43	39	0.0005 − 0.0040	0.0020	1992.7491 − 2688.3502
0 3 3 0 1 f	3 − 38	34	0.0005 − 0.0051	0.0028	1992.7516 − 2536.7277
0 3 3 3 1 e	4 − 42	34	0.0007 − 0.0039	0.0022	8806.7913 − 9452.4713
0 3 3 3 1 f	4 − 37	30	0.0011 − 0.0050	0.0028	8806.7939 − 9307.9306
1 0 0 0 1 e	0 − 91	83	0.0000 − 0.0066	0.0008	1365.8435 − 4443.9265
1 0 0 0 2 e	0 − 89	85	0.0000 − 0.0052	0.0007	1259.4256 − 4199.4066
1 0 0 1 1 e	0 − 92	87	0.0000 − 0.0068	0.0006	3675.1324 − 6795.6258
1 0 0 1 2 e	0 − 88	85	0.0000 − 0.0049	0.0005	3571.1398 − 6423.8802
1 0 0 2 1 e	0 − 69	70	0.0010 − 0.0016	0.0010	5959.9536 − 7709.1259
1 0 0 2 2 e	0 − 85	82	0.0010 − 0.0036	0.0012	5858.0251 − 8500.5825
1 0 0 3 1 e	0 − 64	64	0.0010 − 0.0015	0.0010	8220.3567 − 9714.9192
1 0 0 3 2 e	0 − 68	67	0.0010 − 0.0015	0.0010	8120.1019 − 9804.7857
1 0 0 5 1 e	0 − 47	46	0.0030 − 0.0060	0.0031	12668.1363 − 13465.7561
1 0 0 5 2 e	3 − 48	41	0.0030 − 0.0077	0.0035	12574.1883 − 13402.0744
1 1 1 0 1 e	1 − 68	68	0.0001 − 0.0023	0.0007	2050.0758 − 3776.4846
1 1 1 0 1 f	1 − 55	53	0.0001 − 0.0057	0.0008	2050.0769 − 3186.4135
1 1 1 0 2 e	2 − 58	55	0.0001 − 0.0014	0.0008	1903.9476 − 3161.2710
1 1 1 0 2 f	2 − 47	46	0.0005 − 0.0019	0.0009	1903.9494 − 2734.2130
1 1 1 1 1 e	1 − 67	66	0.0005 − 0.0034	0.0008	4346.9204 − 6010.2858
1 1 1 1 1 f	1 − 67	66	0.0005 − 0.0037	0.0008	4346.9162 − 6014.1590
1 1 1 1 2 e	1 − 69	68	0.0005 − 0.0032	0.0008	4201.8804 − 5964.5091
1 1 1 1 2 f	1 − 67	67	0.0005 − 0.0036	0.0008	4201.8846 − 5868.0670
1 1 1 2 1 e	1 − 67	66	0.0010 − 0.0010	0.0010	6619.2809 − 8269.5815
1 1 1 2 1 f	1 − 70	67	0.0010 − 0.0012	0.0010	6619.2834 − 8423.3825
1 1 1 2 2 e	1 − 67	67	0.0010 − 0.0028	0.0011	6476.5367 − 8126.5302
1 1 1 2 2 f	1 − 70	70	0.0010 − 0.0063	0.0013	6476.5369 − 8279.9376
1 1 1 3 1 e	1 − 51	42	0.0010 − 0.0023	0.0012	8867.2147 − 9820.4597
1 1 1 3 1 f	1 − 49	45	0.0010 − 0.0020	0.0012	8867.2189 − 9749.7059
1 1 1 3 2 e	1 − 49	46	0.0011 − 0.0038	0.0012	8726.4635 − 9607.2456
1 1 1 3 2 f	2 − 50	46	0.0011 − 0.0050	0.0013	8727.9063 − 9645.0928
1 2 2 0 1 e	9 − 49	23	0.0011 − 0.0018	0.0012	2761.4504 − 3633.1359
1 2 2 0 1 f	8 − 47	31	0.0011 − 0.0150	0.0017	2754.8577 − 3561.6412
1 2 2 0 2 e	9 − 26	8	0.0020 − 0.0020	0.0020	2582.6529 − 2808.8128
1 2 2 0 2 f	9 − 26	7	0.0020 − 0.0021	0.0020	2582.6525 − 2808.8147
1 2 2 1 1 e	2 − 60	52	0.0014 − 0.0037	0.0017	5014.8219 − 6353.4478
1 2 2 1 1 f	2 − 58	51	0.0014 − 0.0043	0.0019	5014.8218 − 6266.5610
1 2 2 1 2 e	2 − 45	40	0.0014 − 0.0026	0.0016	4838.7587 − 5595.3077
1 2 2 1 2 f	2 − 49	38	0.0014 − 0.0039	0.0017	4838.7586 − 5734.4743
1 2 2 2 1 e	2 − 53	49	0.0011 − 0.0029	0.0012	7274.7261 − 8313.1711
1 2 2 2 1 f	2 − 55	52	0.0011 − 0.0017	0.0012	7274.7281 − 8392.4841
1 2 2 2 2 e	2 − 55	52	0.0011 − 0.0024	0.0013	7101.2135 − 8219.1860
1 2 2 2 2 f	2 − 50	47	0.0011 − 0.0035	0.0015	7101.2140 − 8026.5629
1 2 2 3 1 e	9 − 25	7	0.0017 − 0.0018	0.0017	9540.5545 − 9742.7194
1 2 2 3 1 f	9 − 24	7	0.0017 − 0.0018	0.0018	9540.5549 − 9724.6733
1 2 2 3 2 e	8 − 27	14	0.0017 − 0.0018	0.0017	9362.8399 − 9609.8720
1 2 2 3 2 f	7 − 26	15	0.0017 − 0.0018	0.0018	9357.0576 − 9590.3736
1 3 3 2 1 e	3 − 40	25	0.0017 − 0.0024	0.0018	7928.6463 − 8521.9960
1 3 3 2 1 f	3 − 40	24	0.0017 − 0.0026	0.0018	7928.6464 − 8521.9873
1 3 3 2 2 e	4 − 33	27	0.0011 − 0.0036	0.0023	7732.6129 − 8134.4702
1 3 3 2 2 f	4 − 33	27	0.0011 − 0.0048	0.0029	7732.6155 − 8134.4694
1 8 8 1 1 f	35 − 35	1	0.0017 − 0.0017	0.0017	9450.9030 − 9450.9030
2 0 0 0 1 e	0 − 51	52	0.0003 − 0.0003	0.0003	2757.1783 − 3735.2672
2 0 0 0 2 e	0 − 65	66	0.0001 − 0.0015	0.0003	2614.2479 − 4189.8779
2 0 0 0 3 e	0 − 65	65	0.0001 − 0.0033	0.0004	2500.7602 − 4078.7086
2 0 0 1 1 e	0 − 65	66	0.0000 − 0.0010	0.0002	5042.5813 − 6611.7206
2 0 0 1 2 e	0 − 72	73	0.0000 − 0.0021	0.0002	4904.8594 − 6819.5761
2 0 0 1 3 e	0 − 67	67	0.0000 − 0.0018	0.0002	4791.2595 − 6454.3905
2 0 0 2 1 e	1 − 60	59	0.0005 − 0.0011	0.0009	7304.3916 − 8631.8830
2 0 0 2 2 e	0 − 69	67	0.0005 − 0.0016	0.0007	7171.0199 − 8916.6854

Band	Range of J	Nb. of energy levels	Unc. Range	Avg. of Unc.	Range of energy levels
2 0 0 2 3 e	0 − 56	57	0.0010 − 0.0012	0.0010	7056.8639 − 8214.0537
2 0 0 3 2 e	5 − 35	29	0.0003 − 0.0029	0.0009	9423.5275 − 9864.9947
2 0 0 3 3 e	2 − 44	28	0.0010 − 0.0013	0.0010	9299.7610 − 10010.3913
2 1 1 0 1 e	8 − 27	20	0.0011 − 0.0024	0.0013	3480.4472 − 3732.6282
2 1 1 0 1 f	9 − 27	19	0.0011 − 0.0017	0.0011	3487.1981 − 3733.5956
2 1 1 0 2 e	3 − 55	51	0.0001 − 0.0109	0.0006	3285.4403 − 4413.7777
2 1 1 0 2 f	4 − 46	43	0.0011 − 0.0033	0.0012	3288.3994 − 4078.6295
2 1 1 0 3 e	1 − 45	44	0.0011 − 0.0055	0.0013	3128.0899 − 3889.8065
2 1 1 0 3 f	6 − 43	37	0.0011 − 0.0027	0.0012	3142.8827 − 3826.3196
2 1 1 1 1 e	1 − 52	51	0.0005 − 0.0018	0.0007	5727.7587 − 6734.8445
2 1 1 1 1 f	1 − 48	47	0.0005 − 0.0017	0.0007	5727.7629 − 6590.0078
2 1 1 1 2 e	1 − 55	55	0.0005 − 0.0017	0.0006	5559.2934 − 6682.5682
2 1 1 1 2 f	1 − 55	55	0.0005 − 0.0015	0.0006	5559.2944 − 6685.6383
2 1 1 1 3 e	1 − 53	52	0.0005 − 0.0017	0.0006	5406.7995 − 6452.1156
2 1 1 1 3 f	1 − 54	52	0.0005 − 0.0030	0.0008	5406.8036 − 6494.6162
2 1 1 2 1 e	1 − 46	40	0.0010 − 0.0043	0.0012	7976.6084 − 8760.5051
2 1 1 2 1 f	2 − 51	39	0.0010 − 0.0040	0.0013	7978.0662 − 8941.1357
2 1 1 2 2 e	1 − 63	62	0.0010 − 0.0041	0.0011	7812.3730 − 9271.0619
2 1 1 2 2 f	1 − 60	57	0.0010 − 0.0019	0.0011	7812.3754 − 9140.0982
2 1 1 2 3 e	1 − 56	55	0.0010 − 0.0018	0.0010	7660.7226 − 8817.7830
2 1 1 2 3 f	1 − 52	50	0.0010 − 0.0027	0.0011	7660.7237 − 8662.6350
2 2 2 1 1 e	3 − 55	42	0.0010 − 0.0026	0.0014	6409.9895 − 7534.8650
2 2 2 1 1 f	3 − 25	18	0.0017 − 0.0025	0.0019	6409.9895 − 6644.1362
2 2 2 1 2 e	3 − 73	51	0.0010 − 0.0031	0.0014	6215.4779 − 8187.6136
2 2 2 1 2 f	3 − 35	29	0.0017 − 0.0025	0.0018	6215.4780 − 6672.8150
2 2 2 1 3 e	2 − 50	44	0.0010 − 0.0031	0.0014	6031.2460 − 6964.3008
2 2 2 1 3 f	2 − 28	22	0.0017 − 0.0018	0.0018	6031.2459 − 6327.0191
2 2 2 2 2 e	5 − 45	36	0.0011 − 0.0031	0.0012	8462.3978 − 9204.0100
2 2 2 2 2 f	2 − 43	31	0.0011 − 0.0018	0.0012	8453.6642 − 9139.3721
3 0 0 0 1 e	3 − 27	25	0.0010 − 0.0020	0.0010	4172.3395 − 4447.1881
3 0 0 0 2 e	0 − 54	55	0.0001 − 0.0020	0.0005	3987.5967 − 5080.4741
3 0 0 0 3 e	0 − 50	51	0.0001 − 0.0010	0.0002	3856.7644 − 4792.5262
3 0 0 1 1 e	0 − 70	70	0.0010 − 0.0016	0.0010	6429.1719 − 8249.8435
3 0 0 1 2 e	0 − 83	80	0.0003 − 0.0022	0.0007	6254.5904 − 8797.3658
3 0 0 1 3 e	0 − 83	81	0.0002 − 0.0022	0.0007	6127.7813 − 8662.8739
3 0 0 1 4 e	0 − 71	71	0.0006 − 0.0012	0.0010	5993.5823 − 7861.7690
3 0 0 2 2 e	3 − 37	32	0.0005 − 0.0013	0.0007	8501.8048 − 9006.7226
3 0 0 2 3 e	2 − 42	40	0.0005 − 0.0013	0.0006	8376.3986 − 9027.0713
3 0 0 2 4 e	7 − 32	17	0.0010 − 0.0012	0.0010	8258.2346 − 8621.7103
3 1 1 0 3 e	12 − 49	20	0.0030 − 0.0030	0.0030	4562.2856 − 5405.3103
3 1 1 0 4 e	2 − 58	57	0.0020 − 0.0034	0.0021	4342.0294 − 5600.2067
3 1 1 0 4 f	1 − 44	33	0.0020 − 0.0025	0.0020	4340.5608 − 5072.2893
3 1 1 1 1 e	1 − 67	63	0.0011 − 0.0028	0.0012	7123.3779 − 8789.3006
3 1 1 1 1 f	1 − 63	60	0.0011 − 0.0023	0.0012	7123.3822 − 8603.9812
3 1 1 1 2 e	1 − 72	69	0.0011 − 0.0055	0.0014	6928.3093 − 8844.8662
3 1 1 1 2 f	1 − 76	69	0.0011 − 0.0150	0.0016	6928.3118 − 9069.6429
3 1 1 1 3 e	1 − 74	69	0.0011 − 0.0064	0.0014	6763.4044 − 8784.5915
3 1 1 1 3 f	1 − 64	61	0.0011 − 0.0026	0.0012	6763.4064 − 8283.8628
3 1 1 1 4 e	1 − 57	56	0.0010 − 0.0017	0.0011	6598.4373 − 7806.3515
3 1 1 1 4 f	1 − 63	60	0.0011 − 0.0023	0.0012	6598.4394 − 8077.0350
3 2 2 0 4 e	4 − 59	34	0.0021 − 0.0021	0.0021	4971.8332 − 6273.2620
3 2 2 0 4 f	9 − 62	33	0.0021 − 0.0023	0.0021	4997.7368 − 6407.9057
3 2 2 1 1 e	2 − 49	43	0.0010 − 0.0024	0.0012	7812.5635 − 8709.8945
3 2 2 1 1 f	2 − 43	41	0.0010 − 0.0036	0.0015	7812.5635 − 8505.4690
3 2 2 1 2 e	3 − 50	45	0.0017 − 0.0033	0.0018	7599.2614 − 8528.9869
3 2 2 1 2 f	3 − 56	49	0.0013 − 0.0040	0.0020	7599.2612 − 8764.2334
3 2 2 1 3 e	2 − 60	51	0.0011 − 0.0028	0.0018	7403.7187 − 8741.2730
3 2 2 1 3 f	2 − 50	48	0.0017 − 0.0035	0.0020	7403.7186 − 8335.3655
3 2 2 1 4 e	2 − 52	41	0.0011 − 0.0028	0.0017	7212.8681 − 8222.4735
3 2 2 1 4 f	3 − 57	37	0.0017 − 0.0040	0.0020	7215.0715 − 8423.7931
4 0 0 0 5 e	36 − 56	14	0.0021 − 0.0025	0.0021	5425.1265 − 6110.8390
4 0 0 1 1 e	0 − 52	53	0.0010 − 0.0017	0.0010	7830.1936 − 8841.8785
4 0 0 1 2 e	0 − 62	63	0.0005 − 0.0012	0.0008	7625.5519 − 9053.7986
4 0 0 1 3 e	0 − 78	78	0.0005 − 0.0016	0.0008	7465.0986 − 9706.8034
4 0 0 1 4 e	0 − 63	64	0.0005 − 0.0010	0.0006	7338.7755 − 8806.6931
4 0 0 1 5 e	0 − 67	63	0.0005 − 0.0012	0.0009	7181.2141 − 8848.8219
4 1 1 0 1 e	8 − 49	35	0.0010 − 0.0019	0.0010	6332.5294 − 7209.2689
4 1 1 0 3 e	15 − 57	21	0.0010 − 0.0011	0.0010	5976.5605 − 7102.1309
4 1 1 0 4 e	6 − 67	53	0.0010 − 0.0014	0.0010	5734.9692 − 7391.8487
4 1 1 0 5 e	24 − 57	9	0.0020 − 0.0021	0.0020	5761.7669 − 6758.7959
4 1 1 1 1 e	5 − 38	29	0.0011 − 0.0022	0.0012	8541.5124 − 9073.8383
4 1 1 1 1 f	5 − 39	31	0.0011 − 0.0019	0.0012	8541.5635 − 9105.0090
4 1 1 1 2 e	1 − 56	50	0.0010 − 0.0027	0.0012	8311.3431 − 9476.5311
4 1 1 1 2 f	2 − 58	54	0.0010 − 0.0015	0.0011	8312.8118 − 9566.1302
4 1 1 1 3 e	1 − 66	59	0.0007 − 0.0026	0.0012	8124.3083 − 9734.2354
4 1 1 1 3 f	1 − 68	62	0.0007 − 0.0038	0.0014	8124.3075 − 9839.2444
4 1 1 1 4 e	1 − 57	54	0.0007 − 0.0020	0.0011	7957.7658 − 9161.9376
4 1 1 1 4 f	3 − 55	51	0.0007 − 0.0030	0.0013	7961.4266 − 9084.1082
4 1 1 1 5 e	1 − 52	44	0.0011 − 0.0017	0.0012	7778.1931 − 8786.2623
4 1 1 1 5 f	4 − 50	45	0.0011 − 0.0020	0.0012	7784.8259 − 8715.3066
4 2 2 0 2 e	12 − 40	19	0.0011 − 0.0011	0.0011	6829.2595 − 7377.3039
4 2 2 0 2 f	9 − 36	14	0.0011 − 0.0012	0.0011	6804.8647 − 7263.7893
4 2 2 0 4 e	11 − 56	20	0.0011 − 0.0017	0.0011	6407.1734 − 7535.9426
4 2 2 0 4 f	11 − 46	14	0.0011 − 0.0011	0.0011	6407.1721 − 7156.2429
4 2 2 1 2 e	2 − 24	15	0.0017 − 0.0022	0.0018	8991.3899 − 9209.1369
4 2 2 1 2 f	2 − 26	20	0.0017 − 0.0023	0.0018	8991.3899 − 9246.5826
4 2 2 1 3 e	2 − 39	30	0.0017 − 0.0023	0.0018	8780.9258 − 9349.8868
4 2 2 1 3 f	2 − 45	28	0.0017 − 0.0030	0.0019	8780.9258 − 9536.5767
4 2 2 1 4 e	2 − 37	19	0.0017 − 0.0019	0.0018	8585.6536 − 9098.6729
4 2 2 1 4 f	2 − 30	28	0.0017 − 0.0019	0.0018	8585.6536 − 8924.3010
4 2 2 1 5 f	8 − 20	12	0.0017 − 0.0032	0.0019	8408.7969 − 8536.7997
5 0 0 0 3 e	1 − 51	51	0.0010 − 0.0012	0.0010	6596.4069 − 7571.2185
5 0 0 0 4 e	0 − 60	52	0.0010 − 0.0030	0.0010	6442.9762 − 7782.8251
5 0 0 0 5 e	1 − 54	40	0.0010 − 0.0015	0.0010	6307.0880 − 7397.1086
5 0 0 0 6 e	2 − 37	29	0.0010 − 0.0013	0.0010	6131.8625 − 6649.5142
5 0 0 1 2 e	2 − 41	37	0.0010 − 0.0023	0.0011	9015.3934 − 9644.3095
5 0 0 1 3 e	1 − 49	45	0.0010 − 0.0013	0.0010	8820.6254 − 9713.5475
5 0 0 1 4 e	0 − 57	51	0.0005 − 0.0012	0.0008	8672.6893 − 9873.3666
5 0 0 1 5 e	0 − 50	47	0.0005 − 0.0014	0.0007	8535.2998 − 9465.4914
5 0 0 1 6 e	3 − 40	25	0.0010 − 0.0019	0.0011	8361.1899 − 8958.8273
5 1 1 0 2 e	8 − 50	31	0.0010 − 0.0010	0.0010	7527.2603 − 8439.2338
5 1 1 0 5 e	36 − 39	4	0.0011 − 0.0011	0.0011	7413.5719 − 7497.4103
5 1 1 0 5 f	33 − 36	4	0.0011 − 0.0011	0.0011	7338.4189 − 7416.0128
5 1 1 1 2 f	35 − 35	1	0.0011 − 0.0011	0.0011	7389.2686 − 7389.2686
5 1 1 1 4 e	4 − 27	11	0.0011 − 0.0017	0.0013	9321.2887 − 9589.3043
5 1 1 1 4 f	9 − 28	9	0.0012 − 0.0012	0.0012	9346.9260 − 9611.0145
5 1 1 1 5 e	8 − 33	8	0.0011 − 0.0014	0.0012	9167.2343 − 9550.3074
5 1 1 1 5 f	14 − 35	8	0.0012 − 0.0014	0.0013	9217.9699 − 9602.8451
6 0 0 0 4 e	3 − 39	34	0.0010 − 0.0013	0.0010	7811.5569 − 8379.3773
6 0 0 0 5 e	3 − 47	41	0.0010 − 0.0016	0.0010	7668.1859 − 8489.0245
6 0 0 0 6 e	5 − 34	11	0.0010 − 0.0010	0.0010	7521.5189 − 7948.5117